

# On the use of nominally anhydrous minerals as phenocrysts in volcanic rocks: A review including a case study from the Carpathian–Pannonian Region

Zsófia Pálos<sup>1</sup>, István János Kovács<sup>2\*</sup>, Dávid Karátson<sup>3</sup>, Tamás Biró<sup>3</sup>,  
Judit Sándorné Kovács<sup>4</sup>, Éva Bertalan<sup>5</sup>, Anikó Besnyő<sup>5</sup>, György Falus<sup>1,5</sup>,  
Tamás Fancsik<sup>5</sup>, Martina Tribus<sup>6</sup>, László Előd Aradi<sup>1</sup>, Csaba Szabó<sup>1</sup>,  
Viktor Wesztergom<sup>2</sup>

<sup>1</sup>Lithosphere Fluidum Research Lab, Department of Petrology and Geochemistry, Eötvös University, Budapest, Hungary

<sup>2</sup>Geodetic and Geophysical Institute, Hungarian Academy of Sciences, Sopron, Hungary

<sup>3</sup>Department of Physical Geography, Eötvös Loránd University, Budapest, Hungary

<sup>4</sup>Department of Physics and Chemistry, Hungarian Institute for Forensic Sciences, Budapest, Hungary

<sup>5</sup>Department of Geochemistry and Laboratory, Mining and Geological Survey of Hungary, Budapest, Hungary

<sup>6</sup>Institute of Mineralogy and Petrography, University of Innsbruck, Innsbruck, Austria

Received: July 7, 2018; accepted: January 8, 2019

The past decade has seen a great number of studies dealing with magmatic water contents and how these could be retrieved by the nominally anhydrous minerals' (NAMs) trace structural hydroxyl (water) contents. Constraints have been made to magmatic hygrometry with clinopyroxene and plagioclase. Although results suggest that the method is more flexible and reliable than melt inclusion studies, they also indicate that the trace hydroxyl contents could still be overprinted by syn- and post-eruptive processes. Clinopyroxenes can hold more structural hydroxyl than plagioclases. A comprehensive review is presented with the inclusion of all published results so far to compile the available pieces of information. As a case study, micro-FTIR measurements are made of a representative set of plagioclase phenocrysts from the Börzsöny Mts. (Carpathian–Pannonian Region). The samples were selected to represent the progress of the volcanic activity in time and space, considering the petrologic and geochemical evolution of volcanic products in well-defined volcanostratigraphic positions. The syn- and post-eruptive cooling rate seems to have the greatest effect on water retention. This means that the systematic investigation of water in volcanic phenocrysts can contribute to distinguish the slowly and rapidly cooling parts of the volcanostratigraphic units.

**Keywords:** micro-FTIR, nominally anhydrous minerals, plagioclase, clinopyroxene, structural hydroxyl, water, cooling rate, lava dome, lava flow, pyroclastic rocks

\*Corresponding author: István János Kovács; Geodetic and Geophysical Institute, Hungarian Academy of Sciences, Csatkai Endre u. 6–8., H-9400 Sopron, Hungary

E-mail: [kovacs.istvan.janos@csfk.mta.hu](mailto:kovacs.istvan.janos@csfk.mta.hu)

This is an open-access article distributed under the terms of the [Creative Commons Attribution-NonCommercial 4.0 International License](https://creativecommons.org/licenses/by-nc/4.0/), which permits unrestricted use, distribution, and reproduction in any medium for non-commercial purposes, provided the original author and source are credited, a link to the CC License is provided, and changes – if any – are indicated.

## Introduction

Magmatic volatile content is an important feature, which affects several properties of magmas, such as mineral assemblage, density and viscosity (Ochs and Lange 1999; Wallace 2005; Giordano et al. 2008; Grove et al. 2012), as well as melting and crystallization (Gaetani and Grove 1998; Danyushevsky 2001). These properties are significant regarding the quality of the magma and volcanic processes, since volatile-rich magmas may trigger explosive eruptions, while volatile-poor ones tend to come to the surface through effusive volcanism (Burnham 1985; Dingwell 1996; Sparks 2003). Of the properties listed above, water plays a key role in magma genesis and eruptive processes, thus, obtaining further knowledge of its role is an essential task. Constraints determining the magmatic water contents are made mostly through olivine-hosted melt inclusion analyses, which can provide estimation on the pre-eruptive water content, but only if there are olivine phenocrysts present. However, water contents from olivine-hosted melt inclusion are not as reliable recorders of the melt water content as previously thought (Lloyd et al. 2013; Plank et al. 2013), because degassing and magma stalling during ascent can influence water contents in inclusions (Portnyagin et al. 2008; Bucholz et al. 2013; Plank et al. 2013; Le Voyer et al. 2014), just as the post-eruptive processes, including slow cooling, induced diffusive water loss (Lloyd et al. 2013). Often there are not enough inclusion-bearing phenocrysts in intermediate and silicic rocks to achieve an analytically as well as statistically robust survey.

If there are no olivine phenocrysts present, another method toward estimating the magmatic water contents is the measurement of structural hydroxyl content in nominally anhydrous minerals (NAMs; Aines and Rossman 1984; Rossman 2006). NAMs can contain structural hydroxyl and molecular water ( $\text{OH}^-$  and  $\text{H}_2\text{O}$ ) in trace amounts (Johnson 2006). The structural hydroxyl and molecular water content in NAMs of volcanic rocks are a focus of scientific interest since the last decade, when several studies quantified the structural hydroxyl and molecular water content using either Fourier-transformation infrared spectrometry (FTIR; Nazzareni et al. 2011; Okumura 2011; Hamada et al. 2011, 2013; Weis et al. 2015; Shepherd and Johnson 2016; Turner et al. 2017) or other methods such as secondary ion mass spectrometry (SIMS; Wade et al. 2008; Lloyd et al. 2016).

NAMs, however, can lose their representative pre-eruptive water contents through diffusional dehydration caused by hot emplacement and slow cooling of lava and tephra (Lloyd et al. 2016; Biró et al. 2016, 2017), degassing of the magma at different levels of the magmatic plumbing system (Hamada et al. 2011) and oxidation (Weis et al. 2015). In addition, pre-eruptive water contents can be overprinted by weathering or hydrothermal alterations (Shepherd and Johnson 2016).

The first part of this paper presents a comprehensive review on the research history of magmatic water content characterization through NAMs, to obtain a well-defined framework in which our results could be interpreted. We pay attention not only to the data obtained, but to the tectonic, petrologic, genetic, and methodological details, which could all influence the results.

As a case study, the water concentrations of plagioclase phenocrysts are analyzed from some representative and stratigraphically as well as geochemically well-studied localities from the Western Segment of Carpathian–Pannonian Region (CPR): the Börzsöny Mts. (Hungary). The samples were chosen to represent the complete volcanic evolution and include products from different volcanic facies from pyroclastic to subvolcanic rocks (Table 1).

The purpose of this research is to assess magmatic water contents using micro-FTIR spectrometry in plagioclase crystals. In this study, “water” and “structural hydroxyl” contents in NAMs are always expressed as molecular water equivalent in wt. ppm if it is not explicitly otherwise specified. With the involvement of whole-rock geochemistry [inductively coupled plasma optical-emission spectrometry (ICP-OES) and inductively coupled plasma mass spectrometer (ICP-MS)] and petrographic description, we expected to investigate any correlation between water contents and geochemical proxies. The bulk geochemistry provides a proxy on the evolution of volcanism. Furthermore, the volcanic facies (i.e., slowly or quickly cooling layers) – from where feldspars are retrieved – could also have a bearing on the measured water contents. Thus, the usefulness of the FTIR spectra might be in distinguishing the samples with distinct origins of volcanic facies or cooling history.

## **Overview of the previous results on the water content of NAMs in volcanic rocks**

Before summarizing the case study results, it is worth reviewing the outcomes of similar studies targeting feldspar and clinopyroxene phenocrysts in different volcanic rocks. The main aim of this section is to give a comprehensive overview with special respect to the estimated magmatic water contents. This will also provide a framework to interpret our results (Table 2).

### *Clinopyroxene*

In the pioneering paper of Wade et al. (2008), the magmatic water contents were published from “rapidly quenched” rocks of four distinct volcanic arcs. The water contents were measured using SIMS in clinopyroxenes. The water contents of the phenocrysts were compared to the concentration of water in olivine-hosted melt inclusions (Wallace 2005). Clinopyroxene phenocrysts showed “water” contents between ~40 and 1,200 wt. ppm; the related calculated magmatic water contents were 0.5–7 wt.%, while the olivine melt inclusions showed 0.1–7 wt.%. Using the data above, a partitioning coefficient has been calculated, ( $D_{\text{H}_2\text{O}}^{\text{cpx/liq}}$  ranging from 0.005 to 0.03), which is linearly proportional to the fraction of the Al-occupied tetrahedral site reinforcing the role of the major element composition in the water-bearing capability of clinopyroxene through coupled substitution, presented by Hauri et al. (2006) and O’Leary et al. (2010).

Table 1  
Sample number, sampling place, genetics and K–Ar age of the samples, based on Karátson (2007)

No.	Location	Genesis	Paleomagnetic group*	Number*	K–Ar age*	Period	H <sub>2</sub> O (ppm)		Magmatic water (wt.%)	
							“wet”	“dry”	“wet”	“dry”
1	Nagy-Hideg-hegy	Lava flow	Normal non-rotated	5	14.7 ± 0.6	3	413.0	340.8	5.2	4.3
2	Kálvária-domb, west from Nógrád Castle-hill	Lava dome	Normal rotated	2	–	1	67.6	52.4	0.8	0.7
3	Magyarkút	Ignimbrite	Reverse non-rotated	XI	14.2 ± 0.9	2	52.2	43.1	0.7	0.5
4	Viski-bérc	Lava flow	–	6	–	3	122.0	55.4	1.5	0.7
5	Pap-hegy	Lava dome	Reverse rotated	4	–	2	252.2	124.6	3.2	1.6
6	Bájdázói kőfejtő	Lava dome root	Normal rotated	I	15.4 ± 0.9	1	25.9	24.8	0.3	0.3
7	Királyrét	Block from ignimbrite	Normal rotated	–	–	1	30.1	28.0	0.4	0.4
8	Nagy-Kő-hegy	Volcanoclastic breccia	–	X/1	15.2 ± 0.8	1	44.2	39.3	0.6	0.5
9	Vilma-pihenő	Block from block and ash flow breccia	Normal non-rotated	–	13.9 ± 0.6	3	150.2	117.0	1.9	1.5
10	Nagy-Pogány-hegy	Subvolcanic	–	–	14.7 ± 0.6	2	90.8	29.4	1.1	0.4
11	Inóci kőfejtő	Lava flow	Normal non-rotated	VI/7	13.7 ± 0.6	3	188.4	155.9	2.4	2.0
12	Hollókő	Block from block and ash flow breccia	–	IV	14.3 ± 1.4	3	64.3	20.6	0.8	0.3

1 – first stage, 2 – second stage, 3 – third stage, with corresponding plagioclase water contents (H<sub>2</sub>O equivalent in wt. ppm), and the calculated melt water contents acquired by the partitioning coefficient of Hamada et al. (2013)

\*Karátson et al. (2000) and references therein

Table 2

## Published literature data of volcanic phenocryst trace water contents and corresponding data

Author and year	Hamada et al. (2013)	Hamada et al. (2011)	Johnson (2005)	Shepherd and Johnson (2016)	Liu et al. (2015)	Nazareni et al. (2008)	Nazareni et al. (2011)	O'Leary et al. (2010)	Okumura (2011)	Wade et al. (2008)	Weis et al. (2015)	Turner et al. (2017)	Lloyd et al. (2016)
Eruption age	–	1986 – 1987	1980 – 1981	1.83 Ma – 484 Ka	24.0 – 10.3 Ma, 8.7 – 0.3 Ma	3930 BP, 2001, 2002	168 – 24 ka	–	1929; 1783; 1914 – 1945	1983; 1723; ~1086; Pleistocene	1949; 1971	1652; 1718	1974; 1977
Sampling place	Rodriguez Triple Junction (Indian ocean rift)	Izu-Oshima (I)	Mount St Helens (USA)	Yellowstone Calderas	North China craton	Mt. Etna (I)	Salina, EoIi Islands (I)	–	Japan Island arc	Galtunggung (RI); Irazu, Arenal (CR); Augustine (USA)	Canary Islands (ES)	Pico Island, Azores (P)	Volcan de Fuego, (GT); Seguin Island, Alaska (USA)
Tectonic environment	MORB	Subduction-related	Subduction-related	Continental hotspot	Destroyed craton	Subduction-related	Subduction-related	–	Subduction-related	Subduction-related	MORB	MORB	Subduction-related
Rock type	Basalt	Low-K tholeiitic basalt	Dacite	Rhyolite	Alkali basalt	Prioritic, alkali basalts	Calc-alkaline basalt, basaltic andesite	Basalt	Andesite	Andesite	Basaltic, ankaramite	Ankaramite	Basaltic andesite
Geneties	Pillow lava	Scoria, lava, bomb	Plinian products and lava dome	Lava flows, tuff	Lava	Lava	Lava rocks	–	Pumice	Scoria lapilli, bomb, hyaloclastite	Lava	Lava, tephra	Subplinian tephra, lava fountain
Phenocryst	plg	plg	plg	plg	cpX	cpX	cpX	cpX	cpX	cpX	cpX	cpX	cpX
Analytical methods	Micro-FTIR, XRF, EMPA, melt inclusion	Micro-FTIR, SEM-EDS, EMPA	FTIR, melt inclusion	FTIR	FTIR, SIMS, EMPA, LA-ICP-MS	FTIR, EMPA, SC-XRD, Mossbauer spectroscopy	FTIR, EMPA, Mossbauer spectroscopy, SC-XRD	experimental petrology	FTIR, EMPA, melt inclusion	SIMS, melt inclusion	FTIR, rehydrating, feldspar hygrometry, EMPA, Mossbauer spectroscopy	SHRIMP-SI, FTIR, EMPA, SIMS, XANES	EMPA, SIMS, EBSD
FTIR	pol	pol	pol	unpol	unpol	pol	pol	–	unpol	–	pol	unpol	–
Absorbance coefficient	Mineral-specific (Johnson and Rossman 2003)	–	Mineral-specific (Johnson and Rossman 2003)	Johnson and Rossman (2003)	(7.09-1 cm <sup>-2</sup> )	Wave number-specific (Libowitzky and Rossman 1997)	Mineral-specific (Bell et al. 1995)	–	Mineral-specific (Auhad et al. 2009)	–	Wave number-specific (Libowitzky and Rossman 1997)	Wave number-specific (Libowitzky and Rossman 1997)	–
H <sub>2</sub> O content (phenocryst, ppm)	<60	20–300	20–200	12–47	13–802	254; 214; 161–254	128–721	51–286	213 ± 36, 247 ± 72, 329 ± 65	~40–1,200	60–100; 200–420	73–687	87–202 (Seguin); 83–495 (Fuego)
D <sub>mineral/melt</sub>	0.01 ± 0.005–0.005 ± 0.005	0.004	0.004	–	4.2 (±0.2) + 6.5 (±0.5)	X <sup>2</sup> WAI – 1.0 (±0.2)	0.290 × (NI)/(V) + 0.00099	0.0228–0.047 (Al-rich); 0.00445–0.0071 (Al-poor)	0.011 ± 0.003	0.005–0.03	0.021–0.045	H <sub>2</sub> O/cpx(0.13 × Al <sup>IV</sup> /cpx) 10,000	0.0228–0.047 (Al-rich); 0.00445–0.0071 (Al-poor)
Melt water content (wt.%)	0.3 (MI) 0.5 – 5.6 (exp)	~7; ~4; ~1	<1–4.6	<1.5	0.58–3.89	–	0.4–0.8; 1.6–2.6; 0.5–3.7	0.9–1.4; 2.9–4.9; 1.3–6.1	3.1; 2.3 ± 0.9; 2.0 ± 0.6	0.3–0.5; 3.0 ± 0.5; 4–5; 4–7	0.71 ± 0.07 – 1.49 ± 0.15	0.28 – 2.2	0.46–1.39 (Seguin)

BP: before present; J: Japan; I: Italy; CR: Costa Rica; RI: Republic of Indonesia; USA: United States of America; P: Portugal; ES: Spain; GT: Guatemala; plg: plagioclase; cpx: clinopyroxene; pol: polarized; unpol: unpolarized; MI: melt inclusion; exp: experimentally determined; EMPA: electron microprobe analysis; SIMS: secondary ion mass spectrometry; XANES: X-ray absorption near-edge spectroscopy; SHRIMP-SI: stable isotope sensitive high-resolution, ion microprobe; SC-XRD: single crystal X-ray diffraction

O'Leary et al. (2010) experimentally defined a partitioning coefficient between high-Ca clinopyroxene and melt for high alumina basalts and nominally alumina-free synthetic ones. The Al content of the melt greatly influences the hydrogen incorporation through two mechanisms: the hydroxyl defects may be coupled to octahedral vacancies and the tetrahedrally coordinated  $Al^{3+}$ -coupled substitution in isolated hydroxyl defects. They used two parametrizations to estimate  $D^{cpx/melt}$ ; in the first case, only the compositional effects are known, and pressure and temperature are unknown, while the second parameterization worked with known pressures and temperatures and thus provided a better fitting expression to experimental data. The authors argue that pre-eruptive water contents of island arc lavas can be better estimated based on clinopyroxene than by using olivine-hosted melt inclusions, since the calculated water contents were systematically higher in the former case.

Water contents of clinopyroxene phenocrysts were also published in the papers of Nazzareni et al. (2008, 2011), collected from Mount Etna (2008) and Salina (2011), respectively. Both papers report polarized infrared measurements. Salina clinopyroxene phenocrysts were evaluated utilizing both the mineral-specific absorption coefficient of Bell et al. (1995) and the wave number-specific one of Libowitzky and Rossman (1997). The water contents of Etna clinopyroxene phenocrysts were evaluated only by the method of Libowitzky and Rossman (1997). The samples were collected from several eruption centers on Salina from basaltic, basalt-andesitic, and andesitic lava flows. On Etna, samples were collected from the picritic 3930 BP eruption and 2001–2002 products of alkali-basalt eruptions. The phenocrysts on Etna contain 161–254 wt. ppm water; the values in Salina are 75–390 wt. ppm. Using the mineral-specific calibration of Bell et al. (1995), higher water contents were yielded than the wave number-specific calibration ones (128–721 wt. ppm). The authors, however, preferred the wave number-dependent absorption coefficient, since the infrared spectra of the pyroxene phenocrysts from Salina were not similar enough to standard (i.e., PMR-53 augite megacryst from Premier Mine, South Africa) published by Bell et al. (1995). The magmatic water contents were determined with the Al content-corrected partitioning coefficient proposed by Wade et al. (2008). The magmatic water contents of Salina in the three distinct eruption centers are 0.4–0.8 wt.%, 1.6–2.6 wt.%, and 0.5–3.7 wt.%, with the calibration of Libowitzky and Rossman (1997), and somewhat higher (0.9–1.4 wt.%, 2.9–4.9 wt.%, and 1.3–6.1 wt.%) with calibration of Bell et al. (1995).

Unpolarized FTIR spectroscopy was applied by Okumura (2011) on clinopyroxene phenocrysts to determine the water contents of three different andesitic magmas of Hokkaido-Komagatake, Asama, and Sakurajima volcanoes, which erupted in 1929, 1783, and 1914–1915, respectively. Samples were collected from fallout pumices from Plinian eruptions for all three volcanoes. Mineral-specific absorption coefficient was applied by Aubaud et al. (2009) to calculate the water content of phenocrysts. The water concentrations in clinopyroxene are  $213 \pm 36$  wt. ppm,  $247 \pm 72$  wt. ppm, and  $329 \pm 65$  wt. ppm, respectively. The magmatic water contents were determined by measuring the clinopyroxene-hosted melt inclusions with FTIR spectrometry.

The melt water contents were 2.8–3.5 wt.%, with an average of  $3.1 \pm 0.4$  wt.%, so a partitioning coefficient was calculated between melt and clinopyroxene, which is  $0.011 \pm 0.003$ .

Liu et al. (2015) measured alkali basalt-hosted clinopyroxene phenocrysts with unpolarized FTIR spectroscopy. They used the absorption coefficient of Bell et al. (1995;  $7.09 \text{ wt. ppm cm}^{-2}$ ); the water concentrations of phenocrysts ranged between 13 and 802 wt. ppm. To constrain the water content of basaltic magma, an experimentally determined partitioning coefficient has been used, which resulted in 0.1–6.3 wt.%.

The magmatic water contents were determined on the Canary Islands basanite and ankaramite lava flows by Weis et al. (2015) using polarized infrared spectroscopy on clinopyroxene phenocrysts. The study was combined with rehydration experiments on the phenocrysts to correct the effects of dehydration during magma ascent or slow cooling. To determine the water content of phenocrysts, both calibrations of Bell et al. (1995) and Libowitzky and Rossman (1997) were applied. However, Bell et al. (1995)'s mineral-specific calibration turned out to overestimate the water contents by 25% because the spectra of the minerals were not similar enough to the standards applied in the mineral-specific calibration. The water concentrations of clinopyroxene were between 18 and 168 wt. ppm before rehydration and 226 and 447 wt. ppm after rehydration. The magmatic water contents were calculated using the rehydrated concentrations and the equation of O'Leary et al. (2010). The resulting values range from 0.84 to 1.49 wt.%.

In the study of Lloyd et al. (2016), clinopyroxene phenocrysts were measured from two geodynamically and geochemically similar eruptions with SIMS (for volatile contents), electron microprobe analysis (EMPA) (for major element composition of pyroxene phenocrysts), photomicrograph (for diffusion analysis), and electron-backscattered diffraction (to determine the orientation of the crystals). The studies were aiming to assess the reliability of clinopyroxene for reconstructing “original” magmatic water contents. To estimate the scale of diffusivity of structural hydroxyl in clinopyroxene, post-eruptive water loss in lava and tephra samples were investigated. The samples were collected from the products of a sub-Plinian eruption, hydrous basaltic andesite tephra of Volcán de Fuego, Guatemala, and a lava fountain-producing eruption of Segoum Island from both tephra and lava flow. In the case of Volcán de Fuego, the phenocrysts contain 83–495 wt. ppm water and the calculated equilibrium melt contains 0.67–3.51 wt.% water. These results appear to differ from the results of melt-inclusion measurements in coevally erupted olivines, which contain 3.4–4.4 wt.% water. The authors explain this discrepancy with diffusive water loss from clinopyroxene. The findings of Lloyd et al. (2016) verify the theory that slowly cooled crystals may have undergone severe post-eruptive water loss by diffusion. The results, on the other hand, are promising for the use of clinopyroxene phenocrysts as a magmatic water recorder in the case of rapidly quenched or cooler magmas, and the diffusion profiles are suitable to assess the “rapid timescales” of the explosive eruptions.

Turner et al. (2017) measured the water contents of clinopyroxene phenocrysts of Azores lavas with micro-FTIR (among other methods). Samples were taken from

ankaramitic lava flows, and tephra units were collected to carry out volatile analysis of olivine-hosted melt inclusions. The FTIR measurements were combined with EMPA, stable isotope sensitive high-resolution, ion microprobe (SHRIMP-SI; to evaluate the data from FTIR), melt inclusion studies with SIMS (to determine a  $D_{\text{cpx/melt}}$  partitioning coefficient), X-ray absorption near-edge spectroscopy (XANES; to determine the  $\text{Fe}^{2+}$ -,  $\text{Fe}^{3+}$ -, or  $\text{Al}^{3+}$ -dependent coupled substitution of structural hydroxyl), and rehydration experiments. The FTIR analyses were carried out using unpolarized infrared radiation, and water concentration data were calculated by the absorption coefficient of Libowitzky and Rossman (1997). The clinopyroxene water contents range from 73 to 687 wt. ppm (124–368 wt. ppm with SHRIMP-SI), whereas the water contents of olivine-hosted melt inclusions range from 0.36 to 0.94 wt.%. With the XANES and FTIR profile measurements, they reinforced that the tetrahedrally coordinated  $\text{Al}^{3+}$  content probably has a greater influence on water concentration zonation than the  $\text{Fe}^{3+}$  content. Based on the reciprocal zonation of Al and structural hydroxyl, diffusive water loss could be excluded. Rehydration experiments also suggested that the clinopyroxene phenocrysts are currently at the maximum of the structural hydroxyl concentration. To determine the pre-eruptive magmatic water content, the  $D^{\text{cpx/melt}}$  partitioning coefficient of Adam et al. (2016) was used. The estimated magmatic water contents range from 0.28 to 2.2 wt.%, where the higher values may provide the more reliable estimation on the pre-eruptive magmatic water contents. Compared to the melt inclusion analyses, clinopyroxenes appear to provide values closer to the original magmatic water content because of their lack of water diffusion.

### *Plagioclase*

Plagioclase phenocrysts of the 1980–1981 eruption of Mount St. Helens were measured with polarized FTIR by Johnson (2005). Water contents of the phenocrysts were ~200 wt. ppm in the early products, while plagioclases from the last dome-forming dacitic lavas contained only 20 wt. ppm water. Thus, the calculated magmatic water contents were 4.6 wt.% in the first Plinian eruptions and less than 1 wt.% at the last lava dome phases.

Hamada et al. (2011) measured plagioclase phenocrysts in the Izu-Oshima volcano's basaltic scoria from the Japan island arc of the 1986–1987 eruptions, which consisted an earlier Strombolian, and later lava flow producing effusive eruptions. The mid-infrared polarized spectra of the plagioclase phenocrysts contain three major bands, approximately at 3,200, 3,400, and 3600  $\text{cm}^{-1}$ . The water contents of phenocrysts ranged from 20 to 300 wt. ppm, the lowest water contents found in the lava samples. The authors used the different water concentrations to model the movements of the magma and the magma chamber system of the volcano. The water contents of the melts were calculated using the partitioning coefficient of Johnson (2005) and turned out to be 7 wt.% in the deepest part (“level 1”) of the system, 4 wt.% in the middle part of the system (“level 2”), and 1 wt.% on the surface (“level 4”).

Hamada et al. (2013) published results of polarized infrared measurements on plagioclase phenocrysts from pillow basalts from the Rodriguez Triple Junction in the Indian Ocean. Plagioclase water contents were estimated using the mineral-specific absorption coefficient of Johnson and Rossman (2003). The spectra displayed three major bands in the mid-infrared region, at 3,200, 3,400, and 3,600  $\text{cm}^{-1}$ . The water contents were usually under 60 wt. ppm in the phenocrysts. Cogenetic melt inclusions were also measured using unpolarized infrared light. From the water content of inclusions, a  $D = 0.01 \pm 0.005$  partitioning coefficient has been calculated but the melt and phenocrysts' hydrogen content showed only a weak correlation. They also published results of hydrous melting experiments for  $D_{\text{H}_2\text{O}}^{\text{plag/liq}}$ , which is 0.008 for melts under 1 wt.% water content, while for over 4 wt.% water content the coefficient is 0.004.

Magmatic water contents of five distinct eruptions of the Yellowstone Volcano were constrained by Shepherd and Johnson (2016) using plagioclase phenocrysts determined by infrared measurements using polarized FTIR. The samples were taken from rhyolitic lava flows and a tuff. The ranges of water contents are 40 and 47 wt. ppm and 12 and 21 wt. ppm for the first caldera and the third caldera, respectively. One sample of the third caldera (Canyon Flow) yielded 760 wt. ppm structural hydroxyl, which is due to hydrothermal alterations. The spectra displayed a stronger, greater half-width band at 3,400–3,500  $\text{cm}^{-1}$  and at the Canyon Flow sample, which is hydrothermally altered, and there appeared a strong and narrower band at around 3,600  $\text{cm}^{-1}$ .

## **Geologic setting and samples**

The samples were collected from the Börzsöny Mountains, which are located at the Western Segment of the CPR (Seghedi et al. 2004; Pécskay et al. 2006). In the CPR Western Segment, volcanism took place in the Middle Miocene (Pécskay et al. 2006). In the Börzsöny Mountains, volcanism occurred from ~16.5 to 13.7 Ma, and it is divided into three eruption periods by Karátson et al. (2000). The underlying strata are from the Middle Miocene (Karpátián–Lower Badenian) sedimentary formations (Egyházasgerge and Nagyoroszi Pebble Formation), which represent shallow submarine environment (Korpás and Lang 1993; Korpás et al. 1998).

The volcanism was initiated in this shallow submarine environment with mostly explosive and dome-forming extrusive eruptions with dacitic chemistry (Karátson et al. 2000). The specialty of the volcanism of this period was the occurrence of garnet-bearing rocks. During this so-called ancient-Börzsöny stage (Karátson 2007), the shallow marine basin was slowly filled, which resulted in subaerial deposition. Based on paleomagnetic measurements the rocks were subject to counterclockwise (CCW) rotation and show normal paleomagnetic polarity (Karátson et al. 2000).

During the second volcanic period, the so-called intermediate stage (Karátson 2007), andesitic lava dome extrusions continued with subordinate dacitic products.

The second period is distinguished from the earlier products based on the reverse paleomagnetic polarity. During the second stage, a rotation of 30° CCW occurred. The garnet-bearing rocks are missing from this period. There are also products of explosive volcanism, an ignimbrite layer of unexplained origin. Due to selective erosion, only few lava flow products are still on the surface; however, the subvolcanic parts of lava domes are exposed. At the end of this period, a large-scale hydrothermal polymetallic ore mineralization affected the coeval and older rocks (Karátson et al. 2000).

The third period lasted from 14.5 to 13.7 Ma and included the formation of the High-Börzsöny lava dome edifice. The eruptions were subaerial, which produced breccias of block and ash flows, lava breccias of the internal parts or the roots of the lava domes, and platy-jointed lava flows, which occurred during the moderate periods of the volcanic activity. The volcanism of Börzsöny ended with a normal paleomagnetic polarity zone (Karátson et al. 2000).

#### *Strategy for selecting the samples*

As previous papers have proven, post-eruptive temperature and cooling history have a great influence on the structural hydroxyl (OH<sup>-</sup>) content of NAMs (Lloyd et al. 2016; Bíró et al. 2016, 2017). At high temperatures (above 600 °C) and pressures, the activity of water is high. However, the activity of water decreases rapidly with pressure, so if the chosen sample is above this temperature for a longer period at atmospheric pressure, most of the hydrogen can be lost under these conditions. Such conditions apply well to thick lava flows and dome structures, which are above 600 °C for a few months, up to years. This permits hydrogen to diffuse out from NAMs on (human) timescales of months to years. On the contrary, if the volcanic rock cools rapidly, there is no significant diffusive hydrogen loss. These favorable conditions occur in thin pyroclastic flow deposits, phreatomagmatic, and Plinian air-fall strata. According to these criteria, the volcanic lithofacies and genetic interpretation add much to the nominally anhydrous plagioclase measurements. Efforts were made to select samples from every lithofacies that occurs in a specific volcanostratigraphic unit.

#### *Volcanological interpretation of samples*

The precise location and stratigraphy of the samples are given in the study of Karátson (2007); in this study, we only provide a shorter description to clarify the processes relevant for the interpretation of the plagioclase water contents (Fig. 1). The interpretation of Karátson (2007) has been fully adapted for this paper. Sample nos. 2, 6, 7, and 8 were collected from the products of the ancient-Börzsöny stage. Sampling site no. 2, Kálvária Hill, is interpreted as an extrusive center (Gyarmati 1976; Korpás et al. 1998) or dacitic lava flow of a lava dome (Karátson 2007). Sample no. 6 from Bajdázó quarry is also (probably root) the part of a garnet-bearing dacite lava dome. Sample nos. 7 and 8 are pyroclastic rocks. Sample no. 7 of Királyrét is a biotite-dacitic clast of a garnet-bearing pumiceous ignimbrite, which was deposited in a shallow-marine

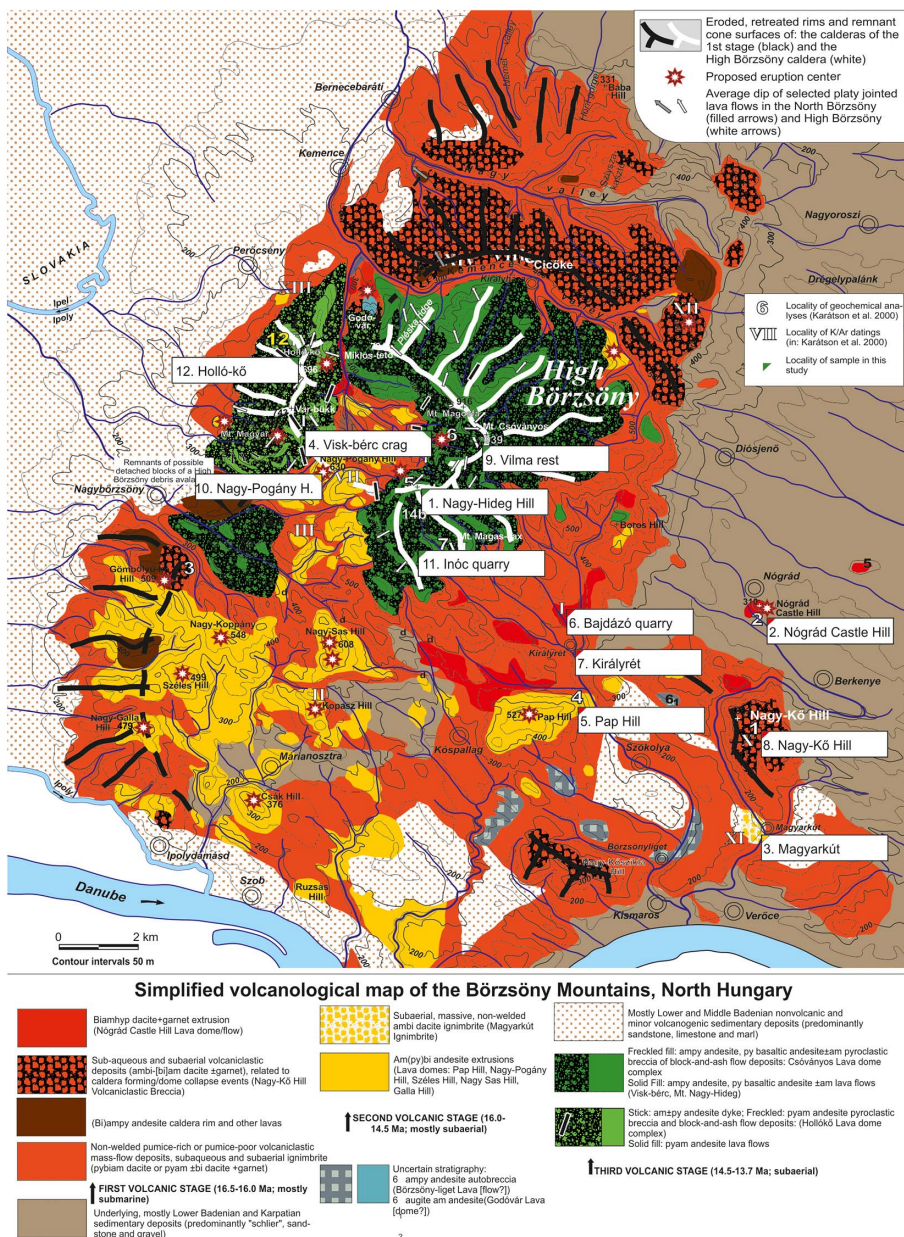


Fig. 1 Geologic map of Börzsöny Mts., with the sampling sites, and corresponding petrology, geochronology, paleomagnetism, and genetics (modified after Karátson et al. 2000)

environment. Sample no. 8 is from the Nagy-Kő Hill, a subaerially redeposited block and ash flow deposit's andesitic block. Field evidence is present, suggesting that the deposits were emplaced hot (e.g., radially jointed-cracked lithoclasts; Figs 1 and 7; Karátson et al. 2000; Karátson 2007).

The samples from the second (intermediate) stage are nos. 3, 5, and 10 (Fig. 1). Sample no. 10 of Nagy-Pogány Hill is from the subvolcanic part of a lava dome complex, with severely altered amphibole phenocrysts and dacitic chemistry. Sample no. 5 was collected at Pap Hill – probably above the paleosurface – deeper part of a lava dome, which also shows alteration of the mafic minerals. Sample no. 3 from Magyarkút is a subaerially deposited pumice-bearing ignimbrite of dacitic lapilli tuff (Karátson 2007), probably also hot-emplaced with the same features as mentioned above.

The rocks that were formed in the third period are andesitic and basaltic-andesitic. Samples collected from this period are nos. 1, 4, 9, 11, and 12 (Fig. 1). Sample no. 12 from Hollókő represents an andesitic block of a valley-filling block and ash flow deposit. Evidence presented in Karátson (2007) shows that the deposit was emplaced hot. The no. 9 Vilma-pihenő rest sample also represents an andesitic block of a probably hot-deposited block and ash flow. Sample nos. 1, 4, and 11 may represent lava flow rocks of slightly different ages and origins. In sample no. 4 Visk-bérc crag, a platy-jointed andesite lava flow was sampled; also, both the no. 1 Nagy-Hideg Hill and the no. 11 Inóc quarry samples represent a platy-jointed basaltic andesite lava flow.

## Methods

### *Petrography*

The petrographic investigations were carried out at Eötvös Loránd University (Budapest), Department of Petrology and Geochemistry, with a Nikon Eclipse LV 100 POL microscope (Japan). Pictures were captured using a Nikon DS-Fi1 digital camera and the attached NIS elements software. We have investigated 30- $\mu$ m-thin sections for petrography, which were provided by Dávid Karátson.

### *FTIR*

Doubly polished 2.5  $\times$  5 cm thin sections were made with a thickness of about 150  $\mu$ m. The thicknesses were measured with a Mitutoyo Digital micrometer with a precision of  $\pm 1$   $\mu$ m in the range of 0–20 mm. The thin sections were removed from the glass slides with acetone. To remove the traces of acetone, the samples were heated for at least 30 min at 90 °C. The unoriented plagioclase phenocryst sections were analyzed by FTIR in the Hungarian Institute of Forensic Sciences, Budapest, using a Bruker Vertex 70 spectrometer coupled with a Bruker Hyperion 2000 infrared microscope. The instrument is equipped with a nitrogen-cooled MCT detector, KBr beam splitters, and Globar light source. Measurements were carried out by unpolarized

light. The spot was a rectangular area with  $60 \times 60 \mu\text{m}$  size. The nominal spectral resolution was  $4 \text{ cm}^{-1}$ . The spectral range was scanned 128 times during each analysis between  $400$  and  $4,000 \text{ cm}^{-1}$ . A more detailed description of the applied micro-FTIR technique are provided in the study of Biró et al. (2016). The unpolarized infrared spectra were collected according to the following considerations: (a) the chosen phenocryst is well exposed, the matrix of the rock does not cover the measured spot; (b) the sampled volume is fresh and free of alterations; and (c) it is also free of accessory minerals or fluid/melt inclusions. To assess the homogeneity of structural hydroxyl content, at least one profile measurement has been carried out per sample.

For the processing of infrared spectra, the OPUS software was used (Bruker, MA, USA). Integration of absorption bands was carried out using the “Integration tool” of OPUS from  $3,052$  to  $3,746 \text{ cm}^{-1}$  with the B method, which integrates only the area above the integration boundaries and the intersection points of spectra.

To estimate the structural hydroxyl content of the phenocrysts, the following equations were applied, where according to the Beer–Lambert law the concentration of the absorbing molecule is proportional to the integrated absorbance [Equations (1) and (2), where  $A_{\text{unpol}}$  is the mean of the unpolarized absorbances and  $A_{a,b,c}$  are the polarized absorbances along the principal crystallographic directions]. In the equations,  $c$  is the concentration of the absorbing molecule (wt.%),  $t$  is the thickness (cm),  $\epsilon$  is the molar absorption coefficient ( $\text{mol/L} \times \text{cm}^{-2}$ )  $202,600 \pm 20,260 \text{ L}/(\text{mol H}_2\text{O} \cdot \text{cm}^2$ ; Mosenfelder et al. 2015),  $M_A$  is the molar weight (g/mol), and  $\rho$  is the density of the mineral (g/L), which is estimated at our case to be  $2,680 \text{ g/L}$  (Libowitzky and Rossman 1997).

$$\bar{A}_{\text{unpol}} = \frac{1}{3}(A_a + A_b + A_c) = \frac{1}{3} A_{\text{pol}}^{\text{tot}}, \quad (1)$$

$$c = \frac{A^{\text{tot}} \cdot M_A}{\epsilon \cdot t \cdot \rho} \quad (2)$$

Using unpolarized infrared radiation, the total polarized absorbance is estimated using the method of Kovács et al. (2008) and Sambridge et al. (2008), where the total polarized absorbance is thrice the average integrated unpolarized absorbance, when the maximum linear unpolarized absorbance is less than 0.15 absorbance unit. For the calculation of the average absorbance spectra, at least 5, but ideally more than 10 unoriented grains are needed, with different orientations with respect to the direction of incoming light. For the calculation of averages, and selecting probably contaminated spectra from measurements, we have set a protocol that provides the best estimation on the real “water contents” of the phenocryst. This protocol or method is described in detail in “Discussion” section. Using polarized infrared radiation on oriented samples was not manageable due to challenges in retrieving whole, large, euhedral plagioclase phenocrysts from

volcanic rocks. To investigate the homogeneity of structural hydroxyl contents, measurements along profiles on individual grains were also performed.

### *Bulk rock chemical analysis*

The bulk chemistry analysis was completed in the Hungarian Mining and Geological Survey. Bulk samples were ground and the  $\sim 63 \mu\text{m}$  fraction was separated by sieve and prepared with  $\text{LiBO}_2$  fusion for chemical analysis. From the pulverized, homogeneous samples, 0.5 g was weighed into platinum crucibles, and then 1.16 g of  $\text{LiBO}_2$  was added. The crucibles were covered with platinum lids and gradually heated in a furnace up to  $1,060^\circ\text{C}$ , fusing the contents for 30 min. After the crucibles had cooled off, they were placed in 100 ml glass beakers, covered with sufficient amount (about 50 ml) of deionized water and 10 ml of 1:1 HCl. Using a magnetic stirrer plate, the fusion melt was dissolved. The solution was transferred into a volumetric flask and filled up to 250 ml. These diluted samples were analyzed with ICP-OES by using a Jobin Yvon Ultima 2C spectrometer. For calibration, a suite of international rock reference materials, and for S and P synthetic solutions, were used. Typically, the precision was  $\pm 2\%$  for Si, Al, Fe, Ca, and Sr, and  $\pm 5\%$  for Ti, Mn, Mg, Na, and K in the detected concentration range of elements. Trace elements, including rare earth elements (REE), were determined by Perkin–Elmer SCIEX ELAN DRC II ICP-MS. The accuracy was  $\pm 2\%$  for Rb, Y, Zr, La, Ce, Pr, Nd, and Pb and  $\pm 5\%$  for Nb, Cs, Sm, Gd, Dy, Er, Yb, and Th. Other elements were of low precision ( $\pm 20\%$ ) due to their low concentration. The element concentrations are expressed as wt.% or wt. ppm, with all the iron expressed as  $\text{Fe}_2\text{O}_3\text{tot}$ .  $\text{CO}_2$  was measured by gas volumetry. Loss on ignition (LOI) was measured gravimetrically at  $1,050^\circ\text{C}$ . The LOI provides information about the amount of  $\text{CO}_2$  and any other volatile component (primarily  $\text{H}_2\text{O}$ ) present in the sample. Therefore, the difference between LOI and data from gas volumetry is marked as  $\text{H}_2\text{O}$ . The element concentrations were recalculated on a volatile-free basis. In the study of Karátson et al. (2000), geochemical data were obtained with XRF, neutron activation analysis and ICP-AES, which were repeated here on the same samples for the sake of comparison. The results are presented in Table 3.

### *EMPA*

The major element composition of plagioclase phenocrysts of the no. 9 (Vilma rest) sample was carried out using a JEOL JXA-8100 electron microprobe, equipped with 5 wavelength dispersive spectrometers (WDX), at the University of Innsbruck (Austria), Institute of Mineralogy and Petrography. Operating conditions were 15 kV acceleration voltage, 10 nA beam current and 20 s peak and 10 s background counting time. A scanning mode with a raster size of approximately  $4 \times 6 \mu\text{m}$  was used. Standards were used in the following order: for Na jadeite, for Mg MgO, for K orthoclase, for Ca diopside, for Mn rhodonite, for Si orthoclase, for Al corundum, for Cr chromite, for Ti rutile, and for Fe almandine.

Table 3  
Bulk rock geochemistry, where available; the data from Karátson et al. (2000) are also presented for comparison

Volcanology, reference	Mt. Nagy-Hideg		Kálvária Hill		Magyarfokt		Vísk-bérc		Pap Hill		Bajdázó quarry		Királyrét		Nagy-Kő Hill		Vilma-phenó		Nagy-Pogány Hill		Inóc quarry		Hollókő	
	Karátson et al. (2000)	Lava flow (2000)	Lava dome (2000)	Lava dome (2000)	Karátson et al. (2000)	Lava flow (2000)	Lava dome (2000)	Karátson et al. (2000)	Lava dome (2000)	Volcanoclastic breccia	Karátson et al. (2000)	Block and ash flow breccia	Subvolcanic	Lava flow (2000)	Karátson et al. (2000)	Block and ash flow breccia	Lava flow (2000)	Block and ash flow breccia						
SiO <sub>2</sub>	57.8	56.7	64.9	66.1	55.7	57.5	56.4	59.1	59.9	62.6	60.6	62.7	59.7	63.8	58.9	63.8	62.7	59.7	63.8	58.9	57.5	61.3	61.3	61.3
TiO <sub>2</sub>	0.90	0.92	0.60	0.57	0.89	0.83	0.82	0.64	0.63	0.54	0.78	0.72	0.71	0.53	0.91	0.53	0.71	0.71	0.53	0.91	0.82	0.70	0.70	0.70
Al <sub>2</sub> O <sub>3</sub>	15.6	18.6	16.6	19.0	16.4	16.5	18.8	15.0	18.2	14.5	17.2	18.5	16.5	15.5	16.0	16.6	18.5	16.5	15.5	16.0	17.9	15.8	15.8	15.8
Fe <sub>2</sub> O <sub>3</sub>	8.55	8.23	4.44	3.92	8.05	8.79	8.36	7.21	7.13	4.18	5.11	5.58	8.08	4.92	8.26	5.28	5.58	8.08	4.92	8.26	7.59	6.83	6.83	6.83
MnO	0.19	0.17	0.05	0.04	0.13	0.14	0.14	0.16	0.16	0.05	0.08	0.07	0.17	0.17	0.12	0.05	0.07	0.17	0.17	0.12	0.15	0.14	0.14	0.14
CaO	7.04	7.79	3.63	5.78	6.62	6.22	7.16	6.64	7.05	9.44	5.55	5.94	6.13	4.44	6.73	6.16	5.94	6.13	4.44	6.73	7.46	5.71	5.71	5.71
MgO	4.07	3.19	1.40	0.93	3.81	3.06	2.78	2.98	2.63	0.98	1.92	1.94	2.36	2.41	2.82	2.10	1.94	2.36	2.41	2.82	3.11	2.01	2.01	2.01
Na <sub>2</sub> O	2.87	3.14	2.54	3.21	1.89	2.68	2.70	2.34	2.92	2.59	2.50	2.92	2.80	3.00	2.70	2.57	2.92	2.80	3.00	2.70	2.93	2.48	2.48	2.48
K <sub>2</sub> O	1.23	1.78	1.94	2.46	0.99	1.68	2.04	1.92	2.73	1.50	1.65	1.09	1.60	1.61	1.67	1.09	2.52	1.60	1.61	1.67	2.26	1.70	1.70	1.70
-H <sub>2</sub> O	0.30	0.30	1.20	1.20	2.31	1.06	0.70	0.70	0.35	0.74	0.39	1.92	0.25	0.27	0.64	1.92	0.25	0.25	0.27	0.64	2.26	0.63	0.63	0.63
LOI	1.05	0.23	0.16	0.16	2.98	1.18	5.40	5.40	0.35	5.38	1.86	2.34	1.15	2.80	0.81	2.34	1.15	1.15	2.80	0.81	2.45	2.45	2.45	2.45
P <sub>2</sub> O <sub>5</sub>	0.19	0.23	0.16	0.16	<0.15	0.18	0.19	0.29	0.35	<0.15	0.15	0.32	0.23	0.19	0.19	0.32	0.18	0.23	0.19	0.19	0.21	<0.15	<0.15	<0.15
SO <sub>3</sub>	<0.15	<0.15	<0.15	<0.15	<0.15	<0.15	<0.15	<0.15	<0.15	<0.15	<0.15	<0.15	<0.15	<0.15	<0.15	<0.15	<0.15	<0.15	<0.15	<0.15	<0.15	<0.15	<0.15	<0.15
BaO	0.06	5.49	0.14	5.34	0.07	0.07	5.16	0.15	1.223	0.06	0.05	5.05	0.13	0.17	0.10	0.05	5.05	0.13	0.17	0.10	980	0.11	0.11	0.11
StO	0.05	4.27	0.05	3.79	0.06	0.04	3.61	0.08	7.25	0.05	0.04	0.05	0.07	0.08	0.06	0.05	3.59	0.07	0.08	0.06	523	0.05	0.05	0.05
La/Yb ratio	7.6	23.7	23.7	23.7	13.2	9.2	16.4	16.4	62.3	62.3	21.7	26.6	14.0	23.8	12.1	26.6	14.0	14.0	23.8	12.1	10.1	10.1	10.1	10.1
Sm	5.1	4.7	5.2	5.2	6.3	5.2	5.0	5.4	4.7	4.7	5.1	4.8	5.5	4.7	4.8	7.0	4.8	5.5	4.7	4.8	5.4	4.6	4.6	4.6
Eu	1.3	1.4	1.3	1.3	1.6	1.3	1.0	1.5	1.2	1.2	1.4	1.4	1.4	1.4	1.3	1.7	1.4	1.4	1.4	1.3	1.2	1.2	1.2	1.2
Gd	4.6	5.0	4.1	4.1	5.2	4.3	4.5	4.5	3.0	3.0	3.9	3.9	4.6	3.7	4.4	4.8	3.9	4.6	3.7	4.4	4.1	4.1	4.1	4.1
Tb	0.8	0.8	0.6	0.6	0.8	0.7	0.7	0.7	0.3	0.3	0.5	0.6	0.7	0.5	0.7	0.6	0.6	0.7	0.5	0.7	0.7	0.7	0.7	0.7
Dy	4.7	4.7	3.2	3.2	4.8	4.5	3.6	3.6	1.3	1.3	2.6	2.9	4.3	2.8	4.2	2.9	4.3	4.3	2.8	4.2	4.2	4.2	4.2	4.2
Ho	1.0	1.0	0.6	0.6	1.0	1.0	0.7	0.7	0.2	0.2	0.5	0.5	0.9	0.6	0.9	0.5	0.9	0.9	0.6	0.9	0.9	0.9	0.9	0.9
Er	3.0	3.0	1.7	1.7	2.7	2.8	2.1	2.1	0.5	0.5	1.3	1.4	2.6	1.6	2.6	1.4	2.6	2.6	1.6	2.6	2.6	2.6	2.6	2.6
Tm	0.5	0.5	0.2	0.2	0.4	0.4	0.3	0.3	0.1	0.1	0.2	0.2	0.4	0.2	0.4	0.2	0.4	0.4	0.2	0.4	0.4	0.4	0.4	0.4

(Continued)

Table 3 (Continued)

Volcanology, reference	Mt. Nagy-Hideg		Káthvária Hill		Magyarkút		Vise-bérc		Pap Hill		Bagdázó quarry		Királyrét		Nagy-Kő Hill		Vilma-pihenő		Nagy-Pogány Hill		Inóc quarry		Hollfőkö	
	Lava flow (2000)	Karátson et al. (2000)	Lava dome (2000)	Lava et al. (2000)	Karátson et al. (2000)	Lava flow (2000)	Lava dome (2000)	Lava et al. (2000)	Karátson et al. (2000)	Lava dome (2000)	Lava dome (2000)	Lava dome root	Ignimbrite	Volcanoclastic breccia	Karátson et al. (2000)	Block and ash flow breccia	Subvolcanic flow	Karátson et al. (2000)	Block and ash flow breccia	Lava flow (2000)	Karátson et al. (2000)	Block and ash flow breccia	Inóc quarry (2000)	Block and ash flow breccia
Yb	2.9	2.9	1.5	2.4	2.7	2.8	1.9	0.4	1.1	1.3	0.8	2.6	1.5	2.5	2.9	2.8								
Lu	0.5	0.5	0.2	0.4	0.4	0.3	0.3	0.1	0.2	0.2	0.1	0.4	0.2	0.4	0.3	0.4								
Hf	4.2	3.8	3.8	3.6	3.4	3.2	3.2	3.2	3.3	3.5	3.7	3.1	3.5	3.5	3.5									
Ta	0.7	0.9	0.9	0.8	0.7	0.7	0.7	0.7	0.8	0.7	0.8	0.7	0.6	0.8	0.8									
W	0.9	1.1	1.0	1.0	1.0	1.8	1.4	1.4	1.1	0.9	2.3	1.4	1.6	1.4	1.4									
Tl	<0.1	0.6	<0.1	0.1	<0.1	<0.1	0.3	0.6	0.6	0.2	<0.1	0.3	<0.1	<0.1	<0.1									
Pb	35.7	13.5	33.7	24.3	24.1	21.5	8.0	23.6	22.5	23.8	21.1	23.9	22.8	27.5	65.2	50.0	25.5							
As	3.4	2.7	2.7	1.9	1.9	2.2	1.9	1.9	2.3	1.9	2.2	2.5	2.2	2.2	2.2									
Rb	69.9	70.0	103.4	58.7	139.3	88.0	82.4	82.0	94.3	96.4	106.0	84.0	81.7	79.3	81.0	93.4								
Y	24.9	29.0	15.1	5.0	23.0	23.0	18.1	22.0	5.3	11.7	13.8	11.0	22.6	14.7	23.5	26.0	23.8							
Zr	124.4	145.0	136.0	141.0	123.5	128.6	145.0	127.0	112.8	126.7	130.0	142.0	146.4	118.9	141.0	138.5								
Nb	8.0	8.0	10.1	10.0	9.6	8.6	9.0	10.0	8.4	9.3	9.8	10.0	9.9	9.6	8.0	8.8								
Mo	0.9	0.7	0.7	0.7	1.0	4.4	4.3	1.5	1.4	1.4	8.5	1.6	5.9	0.9	0.9									
Ag	<0.1	<0.1	<0.1	<0.1	<0.1	<0.1	<0.1	<0.1	0.2	<0.1	<0.1	<0.1	<0.1	0.1	0.1									
Cd	<0.1	<0.1	<0.1	<0.1	<0.1	<0.1	<0.1	<0.1	<0.1	<0.1	<0.1	<0.1	<0.1	<0.1	<0.1									
Sn	1.5	5.0	5.0	2.4	0.9	1.7	2.2	3.4	2.9	2.4	2.4	1.0	1.5	2.4	2.4									
Sb	0.6	0.4	0.4	0.4	0.3	0.4	0.4	0.4	0.4	0.4	0.4	0.5	0.4	0.4	0.4									
Cs	3.3	5.7	4.1	4.3	5.0	6.9	9.7	4.7	4.6	2.2	2.7	6.9	6.9	6.9										
La	22.2	22.1	35.9	31.0	24.8	28.0	31.5	33.7	24.0	24.3	34.0	24.3	36.6	30.3	35.0	28.4								
Ce	43.8	47.0	64.5	58.7	56.4	48.7	53.0	64.8	47.9	47.8	60.0	52.3	64.7	54.6	68.0	51.6								
Pr	5.4	7.4	7.4	7.4	6.0	6.9	5.8	8.4	7.3	7.2	6.3	6.0	6.0	6.0										
Nd	22.3	21.8	27.3	27.0	29.3	23.5	24.0	26.6	28.3	22.9	23.4	33.8	23.7	27.2	25.9	25.0	22.2							
Bi	<0.25	<0.25	<0.25	0.4	<0.25	<0.25	<0.25	<0.25	0.3	<0.25	0.3	<0.25	<0.25	<0.25	<0.25									
Th	8.4	8.0	14.3	10.9	10.8	9.6	10.0	12.1	12.6	8.4	8.7	10.0	9.0	14.0	12.3	14.0	11.7							
U	2.1	3.8	3.8	2.1	2.6	3.2	2.3	2.4	2.9	3.4	3.1	3.3	3.4	3.1	3.3									

Table 3 (Continued)

	Mt. Nagy-Hideg		Kávéfűrés Hill		Magyarokút		Vise-bérc		Pap Hill		Bagdázó quarry		Királyrét		Nagy-Kő Hill		Vilma-sphenó		Nagy-Pogány Hill		Inóc quarry		Hollókő	
Volcanology, reference	Lava flow (2000)	Karátson et al. (2000)	Lava dome	Karátson et al. (2000)	Lava flow	Karátson et al. (2000)	Lava dome	Karátson et al. (2000)	Lava dome	Karátson et al. (2000)	Lava dome root	Lava dome	Ignimbrite	Volcanoclastic breccia	Karátson et al. (2000)	Block and ash flow breccia	Subvolcanic	Lava flow	Karátson et al. (2000)	Block and ash flow breccia	Inóc quarry	Hollókő		
Co	19.7	9.9	16.6	14.6	16.4	11.2	13.0	13.9	15.9	9.9	18.1	11.8	13.0	13.9	15.9	15.9	9.9	18.1	11.8	18.1	11.8	11.8	11.8	
Cr	131.4	40.0	103.6	10.0	88.2	171.0	42.0	261.6	19.0	293.5	78.6	152.8	17.0	395.7	188.7	288.9	63.0	54.9	54.9	63.0	54.9	54.9	54.9	
Cu	21.3	12.1	32.0	128.1	18.7	12.2	8.7	14.2	13.7	10.0	37.7	11.8	13.7	10.0	37.7	11.8	11.8	11.8	11.8	10.0	37.7	11.8	11.8	
Ni	17.5	14.0	5.1	6.0	13.5	2.6	9.0	69.5	7.0	76.8	26.3	27.2	8.0	135.2	9.0	109.2	13.0	4.3	4.3	109.2	13.0	4.3	4.3	
Pb	58.2	24.5	20.9	22.3	20.2	21.3	17.1	23.1	22.3	25.7	20.5	20.5	22.3	25.7	20.5	20.5	20.5	20.5	20.5	25.7	20.5	20.5	20.5	
V	167.2	70.5	147.7	94.5	153.8	51.7	87.4	76.6	111.9	87.8	184.9	118.7	87.8	184.9	118.7	118.7	118.7	118.7	118.7	87.8	184.9	118.7	118.7	
Zn	87.5	51.7	73.1	80.3	63.6	70.9	65.1	70.9	80.4	71.6	71.8	71.8	72.0	71.6	71.8	71.8	71.8	71.8	71.8	72.0	71.6	71.8	71.8	
H <sub>2</sub> O wet	<b>413</b>	<b>68</b>	<b>52</b>	<b>122</b>	<b>252</b>	<b>26</b>	<b>30</b>	<b>44</b>	<b>150</b>	<b>91</b>	<b>188</b>	<b>64</b>	<b>91</b>	<b>188</b>	<b>64</b>	<b>64</b>	<b>64</b>	<b>64</b>	<b>64</b>	<b>91</b>	<b>188</b>	<b>64</b>	<b>64</b>	
H <sub>2</sub> O dry	<b>341</b>	<b>52</b>	<b>43</b>	<b>55</b>	<b>125</b>	<b>25</b>	<b>28</b>	<b>39</b>	<b>117</b>	<b>29</b>	<b>156</b>	<b>21</b>	<b>29</b>	<b>156</b>	<b>21</b>	<b>21</b>	<b>21</b>	<b>21</b>	<b>29</b>	<b>156</b>	<b>21</b>	<b>21</b>	<b>21</b>	

The La/Yb ratio and H<sub>2</sub>O values are specifically highlighted. Gd and W values have non-accredited measurements.

## Results

### *Petrographic description*

Instead of geochronologic order, we describe petrographic features according to the samples' volcanic facies. The following description is justified because the overall geochemical features and the rock types hardly influence the measured water contents of the plagioclase crystals.

### *Samples from lava flows*

The samples from lava rocks are of andesitic composition with microholocrystalline texture. The larger plagioclases are 1 mm long, hypidiomorphic, and with well-defined or blurred (no. 1 Nagy-Hideg Hill) edges. Some show oscillatory zoning, and polysynthetic twinning, with many inclusions in the core. The other phenocrysts in the samples are orthopyroxene, clinopyroxene, amphibole, and opaque minerals as accessory phases (Fig. 2).

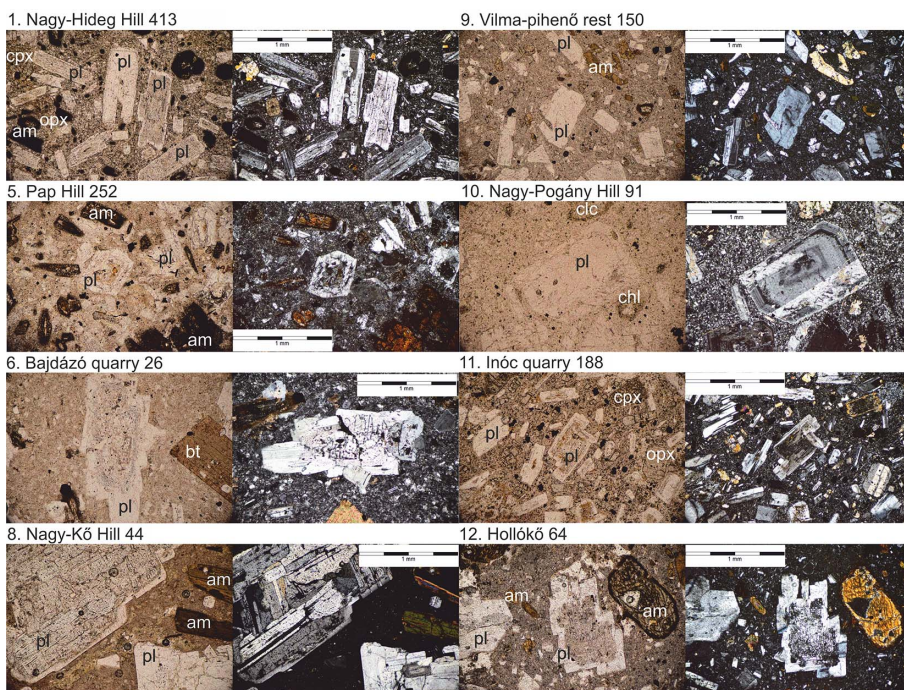


Fig. 2

Photomicrograph of thin sections from the representative samples of Börzsöny Mts. Left: plane-polarized; right: cross-polarized light; Cpx: clinopyroxene; chl: chlorite; clc: calcite; pl: plagioclase; am: amphibole; opx: orthopyroxene; bt: biotite. The phenocryst water content is depicted next to sample name in wt. ppm

### *Lava domes' rocks*

The samples from the lava domes have porphyric texture with hialopilitic (no. 6 Bajdázó quarry) or holocrystalline (no. 5 Pap Hill) matrix. The plagioclase phenocrysts are large, hypidiomorphic and form apr. 3 mm cumulates, with the individual minerals 1–1.5 mm long. They have oscillatory zones, polysynthetic twins, and altered core (no. 5); sometimes, the core is lost during the thin section preparation. The other observable phenocrysts are amphibole, biotite, and as accessory mineral, garnet (no. 6 Bajdázó quarry) occurred (Fig. 2).

### *Subvolcanic rocks*

The no. 10 Nagy-Pogány Hill sample is of subvolcanic origin, with porphyric-microholocrystalline texture. The plagioclase phenocrysts are 1.5 mm large, idiomorphic, with oscillatory zones and polysynthetic twinning. There are altered inclusions and zircon and apatite present as inclusions. Certain zones show resorbed, spongy texture, especially the ones close to the core. The other abundant phenocrysts are amphibole, biotite, quartz, and accessory opaque minerals (Fig. 2).

### *Volcano-sedimentary rocks*

The thin sections of the block and ash flow breccias are made of clasts, so the textures are porphyritic, with hyalopilitic (no. 8 Nagy-Kő Hill) or pilotaxitic–trachytic (no. 9, 12 – Vilma-pihenő rest and Hollókő, respectively) matrix. The plagioclases are hypidiomorphic, 1–2 mm long; they show oscillatory zones and the core is more (no. 9) or less (no. 8) spongy, containing small, more or less altered inclusions. In the case of sample no. 9, the plagioclases show wide polysynthetic twinning. Other phenocrysts are amphibole and biotite. Zircon occurs as accessory phase (sample no. 8). In sample no. 9 (Vilma rest) and no. 12 (Hollókő), other phenocrysts are amphibole, biotite, ortho-, and clinopyroxene (sample nos. 9 and 12; Fig. 2).

### *Bulk rock chemistry*

*Major elements.* The bulk rock major element compositions were plotted on a total alkali silica (TAS) diagram (Fig. 3), where the samples correspond to dacitic and andesitic assemblages. SiO<sub>2</sub> contents decrease from the first volcanic period toward the subsequent ones. The samples from the second volcanic phase show the highest total alkali content. The samples of the third period are andesitic. The polygon outlined by a solid black line shows the reference data from the CPR Miocene calc-alkaline volcanic rocks according to the references cited in Kovács and Szabó (2008) and Karátson et al. (2000). Among the reference data, the samples from the Börzsöny belong to alkali-poorer and SiO<sub>2</sub>-rich intermediate rocks (Karátson et al. 2000).

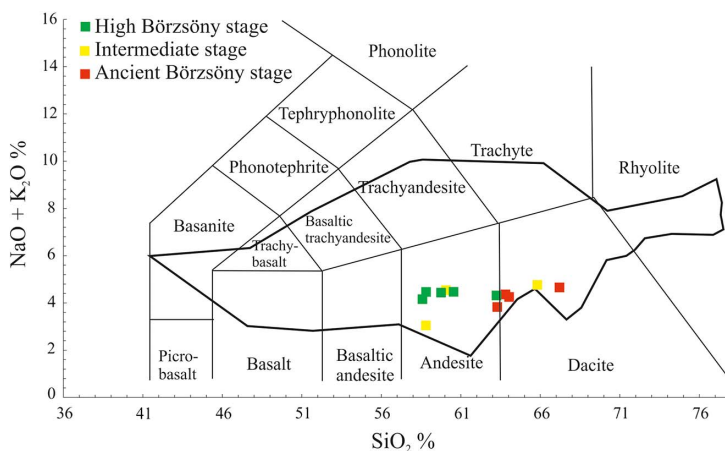


Fig. 3

Total alkali vs. silica diagram after Le Bas et al. (1986) for the CPR's "western segment" Middle Miocene volcanic rocks as a reference field (solid black outline; see Kovács and Szabó 2008 for references) and the Börzsöny samples (squares, with colors corresponding to the stages of volcanic activity: red – first, yellow – second, green – third)

*Trace elements.* The chondrite-normalized REE diagram (Fig. 4) shows a concave-upward pattern (Nakamura 1974) without major anomalies. There is greater enrichment of light rare earth elements (LREEs; La–Eu), than in heavy rare earth elements (HREE; Gd–Lu), relative to chondritic values. The tendency is that the subsequent volcanic periods show a less and less enriched character of LREE and a more enriched character in HREE, compared to the products of earlier volcanic phases. There is greater depletion in HREE in the Bajdázó quarry sample (no. 6). The reference data of the CPR show a similar REE distribution; LREE enrichment is greater and a negative Eu-anomaly is present. The HREE enrichment is slightly more expressed. The La/Yb ratio decreases from the first stage volcanic rocks toward the third stage ones. The La/Yb ratio is above 20 in the first volcanic stage, and at no. 10 Nagy-Pogány Hill, it is also above this value. In the third stage, these ratios are below 15, with the lowest values provided by the latest products (Table 3).

In the trace element diagram normalized to the primitive mantle according to McDonough and Sun (1988), the pattern descends from Cs to Lu (Fig. 4). Generally, the samples from Börzsöny are enriched in large-ion lithophile elements (LILEs) and are mildly depleted in high-field strength elements (HFSEs). As the volcanism evolves, the anomalies flatten, but the products of distinct stages of volcanism do not show significant changes except in a few, special cases. LILE displays a positive anomaly in the samples from the first volcanic period, compared to the rocks of subsequent volcanic periods. During the second volcanic period, Ba, Pb, and Sr show a greater positive anomaly than in the others. Both the positive and negative anomalies flatten in the third period. The reference data taken from the Middle Miocene volcanic

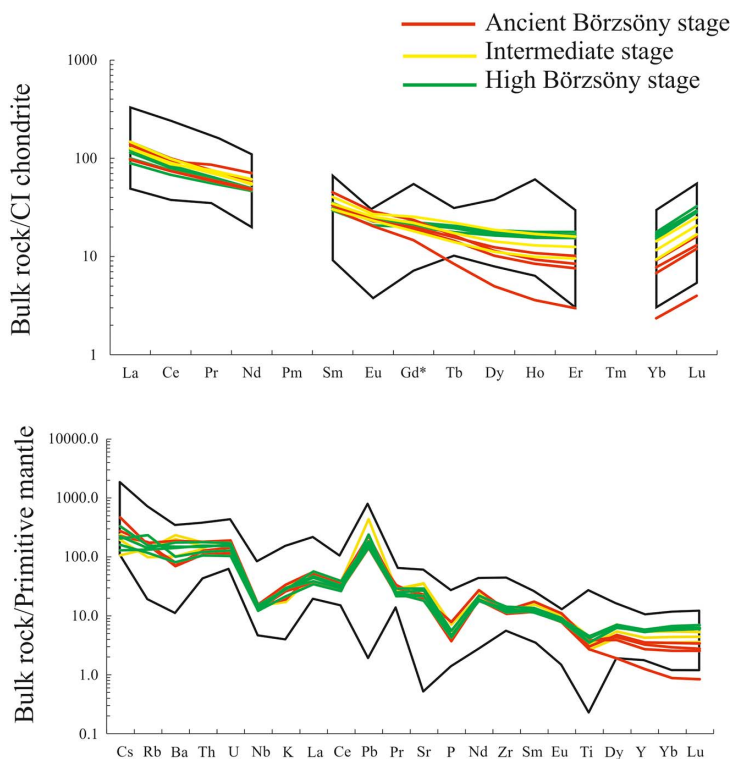


Fig. 4 Chondrite-normalized (Nakamura 1974) rare earth element pattern of the Middle Miocene igneous rocks of the CPR (above) and primitive mantle-normalized (McDonough and Sun 1988) trace element pattern of the Middle Miocene igneous rocks of the “western segment.” Both are plotted with solid outlining; rocks of Börzsöny are colored according to the stages of volcanic activity: red – first, yellow – second, green – third

rocks of the CPR show a similar pattern to the Börzsöny. Generally, the LILEs are more enriched, the HFSEs are more depleted.

*FTIR.* Figure 5 shows the representative average spectra normalized to 1 cm thickness. The results of profile measurements are presented in the Supplementary Material. The infrared spectra provide qualitative information on the location of the absorbing bands, whereas the integrated area of the bands provides quantitative information on the amount of the absorbing species. The major bands are located at (a)  $\sim 2,900$ , (b)  $\sim 3,200$ , (c)  $\sim 3,400$ , and (d)  $\sim 3,620$   $\text{cm}^{-1}$ . The bands at  $\sim 3,200$  and  $\sim 3,400$   $\text{cm}^{-1}$  are abundant in every sample, but their respective intensities vary. The bands belonging to  $\sim 3,620$   $\text{cm}^{-1}$  also do not have uniform heights, but they are narrower than any other bands.

To obtain the average integrated absorbance, two different processing algorithms were applied to the spectra: the “wet” and the “dry” method. With the “dry” method,

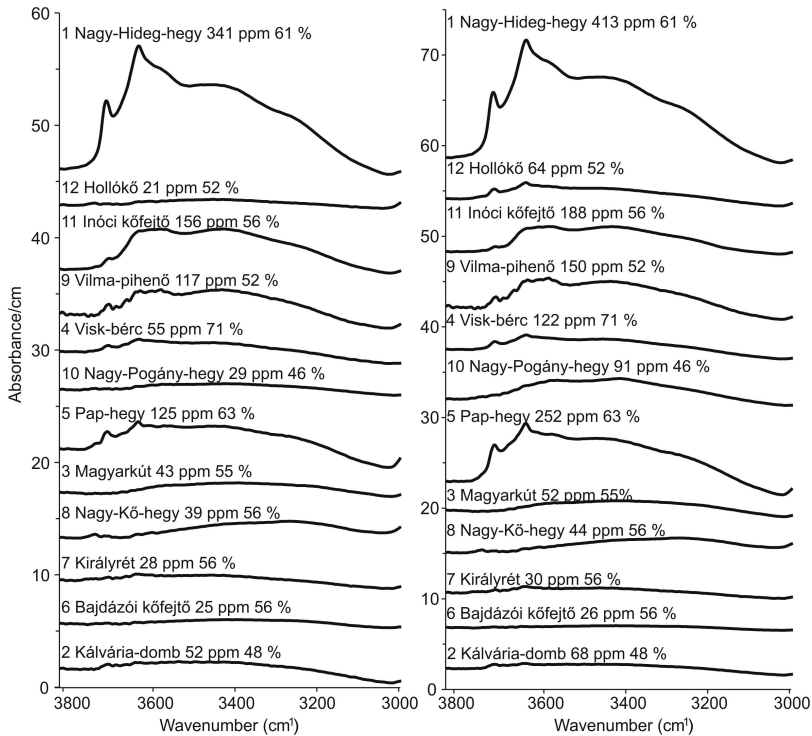


Fig. 5  
Representative average spectra normalized to 1 cm thickness. The “dry” method is to the left, whereas the “wet” method is to the right. The mean anorthite contents are shown for each sample and the calculated water concentrations is in wt. ppm. The “dry” average spectra exclude molecular water and hydrous minerals as much as possible, while the “wet” spectra allow the contribution of altered phases in the water content of plagioclases

only the mean of the integrated absorbances related to the structural hydroxyl bands were included in calculation of concentration by the Beer-Lambert law. The criterion is the following: if the integrated absorbance is no more than thrice that of the minimal absorbance, which is the maximum allowed difference from the anisotropy of structural hydroxyl, and the spectrum contains no bands around  $\sim 3,620\text{ cm}^{-1}$ , the spectrum is considered as “dry.” With the “wet” method, every band’s absorbance was included in the average. With the “dry” selection, structural hydroxyl contents range from 20 to 340 wt. ppm, whereas “wet” estimation gives 26–413 wt. ppm structural hydroxyl contents.

The samples taken from some part of a *lava dome* edifice (nos. 2 and 6; Kálvária Hill and Bajdázó quarry, respectively) show wide, very flat absorbance bands, with only a weak band centered around  $3,400\text{ cm}^{-1}$ ; sample no. 2 (Kálvária Hill) also shows small bands at  $3,620$  and  $3,700\text{ cm}^{-1}$ . They display low water contents, 52 and 24 wt. ppm,

respectively, with the “dry,” and 67 and 26 wt. ppm with the “wet” method. Sample no. 5 from Pap Hill is also a part of a lava dome edifice; however, its spectrum displays higher bands centered at  $3,400\text{ cm}^{-1}$ , with a “shoulder” at  $3,200\text{ cm}^{-1}$ . It also shows high bands (especially at the “wet” spectrum) at  $3,600\text{--}3,700\text{ cm}^{-1}$ , which provided high water content, 124 wt. ppm with the “dry” and 252 wt. ppm with the “wet” method.

The sample that represents a *subvolcanic* rock, no. 10 (Nagy-Pogány Hill), displays in its spectrum flat, low absorbance bands, which are more visible at the “wet” spectrum, centered at  $3,400\text{ cm}^{-1}$  with a shoulder at  $3,600\text{ cm}^{-1}$ . It indicated relatively low water content with the “dry” method: 29 wt. ppm, and high water content with the “wet” method: 90 wt. ppm.

The *lava flow* samples (nos. 1, 4, and 11 – Nagy-Hideg Hill, Visk-bérc crag, and Inóc quarry, respectively) show the highest bands on their spectra;  $3,400\text{ cm}^{-1}$  band is pronounced, with a lower shoulder at  $3,200\text{ cm}^{-1}$ , but there are also high bands belonging to  $3,600$  and  $3,700\text{ cm}^{-1}$ . The no. 4 sample from Visk-bérc crag, however, displays less intense bands. They show high water contents, 340, 55, and 155 wt. ppm, respectively, with the “dry” method (except for Visk-crag), and 412, 122, and 188 wt. ppm, respectively, with the “wet” method.

The samples collected from *pyroclastic* rocks (nos. 8, 3, 7, 9, and 12 – Nagy-Kő Hill, Magyarút, Királyrét, Vilma-pihenő rest, and Hollókő) have spectra that display very low and wide bands, with bands at  $3,400\text{ cm}^{-1}$ . Only sample no. 9 from Vilma-pihenő rest shows higher bands at  $3,400\text{ cm}^{-1}$  and probably overlapping bands at the region of  $3,620\text{--}3,700\text{ cm}^{-1}$ . It is the only sample with high water content: 117 or 150 wt. ppm with the “dry” and “wet” methods, respectively. The no. 7 sample from Királyrét is a dacitic block from an ignimbrite. Its spectrum shows a small, wide band at  $3,400\text{ cm}^{-1}$  and on the “wet” spectrum, there are very small, bands in the region of  $3,620\text{ cm}^{-1}$ . The sample displays low water content: 28 and 30 wt. ppm, respectively, with the “dry” and “wet” methods. The no. 3 sample from Magyarút is a lapilli tuff from an ignimbrite deposit; it shows a wide, flat band at  $3,400\text{ cm}^{-1}$  with a small shoulder at  $3,200\text{ cm}^{-1}$ ; the  $3,620\text{ cm}^{-1}$  band is missing. It has low water content: 43 and 52 wt. ppm, respectively, with the “dry” and “wet” methods. The no. 8 sample from Nagy-Kő Hill is the only one where the  $3,200\text{ cm}^{-1}$  band is higher than any other bands. It contains 39 or 44 wt. ppm water, respectively, with the “dry” and “wet” methods.

Generally, the samples taken from root zones of lava domes, or the ones that belong to volcanoclastic or pyroclastic breccias or the deeper part of the volcanic system, show less intense bands (e.g., sample nos. 2, 3, 6, 7, 8, 10, and 12) than the ones taken from lava flows or the surface of a lava dome (nos. 1, 4, 5, and 11).

As mentioned, profile measurements have been completed where we measured through one or two phenocrysts in length. Along the profiles, great variability was observable in the band intensities, especially the ones at  $\sim 3,620\text{ cm}^{-1}$ . In some places, this variability was not present, however, such as at no. 5 (Pap Hill) and no. 11 (Inóc quarry).

*EMPA.* The plagioclases were analyzed in sample no. 9, collected at Vilma-pihenő rest. The back-scattered electron (BSE) images of idiomorphic minerals show darker (Na-rich) and lighter (Ca-rich) zones (Fig. 6a and b), which are 5–20  $\mu\text{m}$  wide. In some

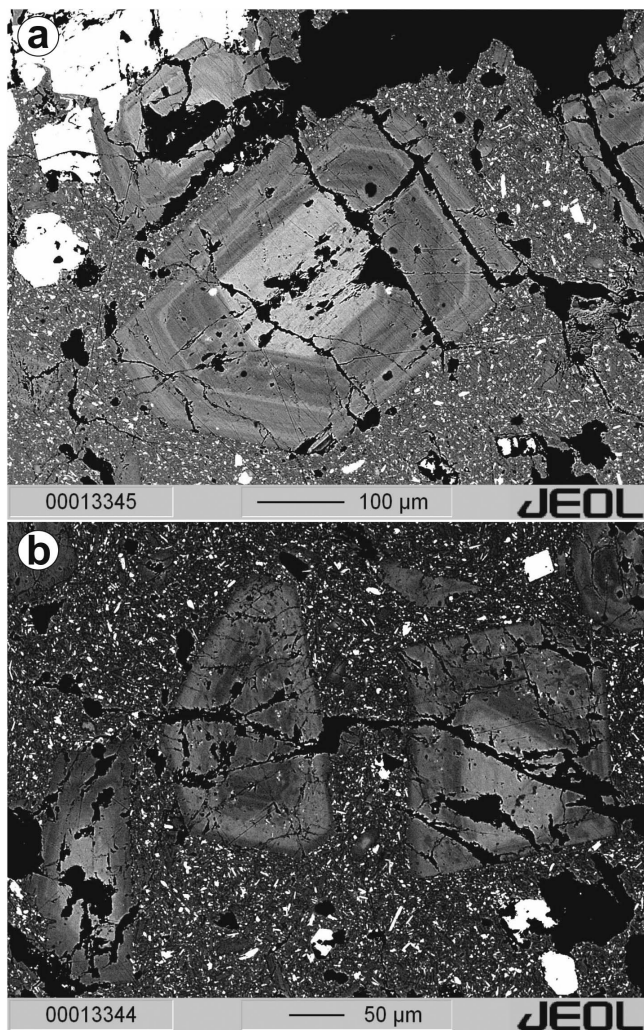


Fig. 6  
Zoned plagioclases from sample no. 9 (Vilma rest)

cases, the cores of the phenocrysts are Na-rich, and become more Ca-rich, with Ca- and Na-rich zones alternating, toward the edges, but sometimes the core is Ca-rich and toward the edges, it becomes Na-rich. Major element compositions show 72%–56% anorthite content, so the feldspars are bytownitic to labradoritic.

## Discussion

### *Major elements*

According to the TAS diagram (Fig. 3; Le Bas et al. 1986), the older volcanic products of the volcanism of Börzsöny Mts. are richer in SiO<sub>2</sub>; after the first dacitic rocks, andesitic ones were formed (Karátson et al. 2000). Since visible variations occur, the bulk rock geochemistry will be discussed according to the age of the rocks, rather than the volcanic facies. Sample no. 10 from Nagy-Pogány Hill, of the second stage, has an increased silica content of 65.82% due to silica-rich hydrothermal alteration, which occurred before the third volcanic stage (Karátson et al. 2000). The samples of the second stage also have high alkali contents for the same reasons. The silica content of the products of the third volcanic stage decreases with time. This suggests that the volcanism became gradually more and more silica- and alkali-poor.

Considering the whole CPR, magmatic rocks show a wider variety, due to distinct scales of assimilation and fractionation and further processes that may have had an influence on the magma genesis. Börzsöny possibly had its own magmatic plumbing system (Harangi et al. 2007), but its evolution and chemical variations resemble the surrounding unit, the Visegrád Mts. (Karátson 2007; Karátson et al. 2007).

### *Trace elements*

The samples are enriched in incompatible trace elements, especially in LREE and LILE. There is a negative anomaly at HFSE. Subduction-related mantle enrichment is a possible explanation for these anomalies (e.g., positive with Ba and Rb and negative with Nb, Zr, and Ti; Saunders et al. 1991)

The chondrite normalized plot (Fig. 4) suggests a magma genesis in the presence of garnet, based on the low concentration and normalized ratio of HREE (Harangi et al. 2001 and references therein). Sample no. 6, taken from Bajdázó quarry (garnet-bearing dacite), is strongly depleted in HREE, which suggests garnet fractionation in this case. Since the garnet is also abundant in the other samples from the first volcanic period, from which the sample no. 6 was also taken, the garnet fractionation is a well-established explanation for the HREE-depleted character. The La/Yb ratio decreased with time, which means a probable attenuation in source melting potential and therefore quasi continuous geochemical depletion.

In the primitive mantle normalized plot (McDonough and Sun 1988), as the volcanism gets younger, both the negative and positive anomalies are attenuated. In the second volcanic period, the anomalously great concentrations of Ba and Pb for some samples do not fit in this scenario; it is possible that secondary alterations could have caused these anomalies (e.g., hydrothermal alterations). With sample no. 10, from Nagy-Pogány Hill, there is an even more significant positive anomaly, suggesting more significant alteration, which is supported by its subvolcanic origin, and by the

petrographic characters as well (e.g., chloritized amphibole pseudomorphs, micro-holocrystalline texture rich in quartz, calcite replacing the plagioclase core).

#### *Major element chemistry of the plagioclase phenocrysts*

The BSE images display normal as well as reverse-zoned phenocrysts. The zoning represents the evolution of magmatic processes; as the plagioclase phenocryst grows, its chemistry tries to maintain equilibrium with the surrounding magma. Thus, the multiple types of zoning suggest that phenocrysts of different evolutions erupted at once. The anorthite content varies from 72 to 56 wt.%, implying the role of differently evolved melts during the crystallization of plagioclase.

#### *FTIR*

Structural hydroxyl (Johnson and Rossman 2003, 2004) appears as a wide absorption band at  $\sim 3,200\text{ cm}^{-1}$  (Mosenfelder et al. 2015). The bands at  $\sim 3,400\text{ cm}^{-1}$  represent the stretching bands of molecular water. Molecular water is not incorporated directly in the crystal lattice of plagioclase; instead, it appears in nano- or microscale inclusions. The rather sharp bands at  $\sim 3,620\text{ cm}^{-1}$  and above usually represent the minerals of secondary alteration, such as clay minerals, sericite, or other hydrous phyllosilicates. Occasionally, due to the lateral resolution of  $60 \times 60\text{ }\mu\text{m}$  of the infrared measurement, sampling some parts of the more altered zones was unavoidable. The distinction of these variably broad and frequently overlapping bands is not always straightforward. Thus, the measured “water” concentration includes contributions from all the listed hydrogen species (e.g., structural hydroxyl, molecular water in inclusions, and also secondary alterations). It follows that a careful evaluation strategy was applied, which is dedicated to decrease the contributions of molecular water in inclusions and secondary alteration products (such as sericite).

The acquired values are in a good agreement with the earlier published structural hydroxyl contents (Johnson and Rossman 2003; Johnson 2005; Hamada et al. 2011, 2013; Mosenfelder et al. 2015; Shepherd and Johnson 2016). The best agreement is shown in the case of plagioclases in a dacitic rock of Mount St. Helens (Johnson 2005) and the plagioclases published by Hamada et al. (2011). The first volcanic period’s structural hydroxyl contents are the lowest, with 24–44 wt. ppm; the second volcanic phase shows medium values with 124 wt. ppm, whereas the third period’s samples show the highest structural hydroxyl content. The average integrated unpolarized absorbances have been calculated, therefore, with two selecting algorithms, called “wet” and “dry” selections. With the “dry” algorithm, the spectra showing strong bands at  $\sim 3,690$  and  $3,620\text{ cm}^{-1}$ , due to hydrous silicates, are omitted, and from the remaining pool of samples, only those spectra are included that have a maximum absorbance of at most thrice that of the minimal absorbance. In this way, we expect to exclude the contribution of secondary alterations and molecular water in inclusions. In addition, the consequence of inhomogeneity in structural hydroxyl content

can be minimized. Thus, the “dry” algorithm provides a robust yet conservative estimation of the structural hydroxyl content in feldspars. With the “wet” algorithm, spectra were omitted only if  $\sim 3,620\text{ cm}^{-1}$  band was intense. This approach, however, still includes molecular water in inclusions and the possible heterogeneity of “structural hydroxyl.”

#### *FTIR profiles – No evidences on diffusion*

According to the petrographic and microprobe analyses, there are several samples where the major elements show oscillatory, normal, or reverse zoning. However, the FTIR profiles (see Supplementary Material) usually do not show any significant zonation. The structural hydroxyl content appears to be homogeneous, apart from inclusion-rich zones with molecular water and secondary alterations. This implies that there are no diffusion profiles, because the structural hydroxyl content is later equilibrated in the phenocrysts. According to the previous studies, the structural hydroxyl content is homogenized in the plagioclase via the relatively quick diffusion of hydrogen (Johnson and Rossman 2013).

#### *Variability of water content with volcanic facies and sampling place*

The bulk rock geochemistry measurements were carried out to assess whether the obtained water contents correlate with the major or trace element components of the products. Since the trace element compositions show a pattern interpretable as a gradually depleting magma source in mobile elements, the plagioclase water contents do not show such a clear trend. There are several samples where the plagioclase water contents turned out to be unusually low (e.g., nos. 2, 3, 6, 7, 8, 10, and 12) compared to their mobile element contents, but there are also a few where the water contents seem to be high (e.g., 1, 4, 5, 9, and 11), despite their lower mobile major and trace element composition. The water contents show better connection with the volcanic facies than the whole rock chemistry or the major element composition of the plagioclase crystals; in some cases, this might reflect effects of hydrothermal alteration. Plank et al. (2013) reported similar discrepancies examining olivine melt-inclusion water contents and comparing with subduction-related elements. To better visualize the volcanostratigraphic positions and the corresponding, supposed cooling rate, samples are presented on an overview figure, with each volcanic activity stage and cooling rates, depicted in Fig. 7.

The samples of the first volcanic period show low water contents, and belong mostly to *lava dome*-forming eruptions or pyroclastic breccias of previously formed lava domes (lava domes: nos. 2 and 6; resedimented breccia of a former lava dome: no. 8 according to Fig. 7; Karátson et al. 2000; Karátson 2007). The rock type of these lava domes is dacitic. The water contents of the plagioclases are low: 24–54 wt. ppm. These low water contents could be the result of the slow cooling of the lava dome rocks, as Johnson (2005) has reported similar results from Mt. Saint Helens. The Királyrét sample (no. 7) is a biotite–dacite block from an *ignimbrite* in which the feldspars also

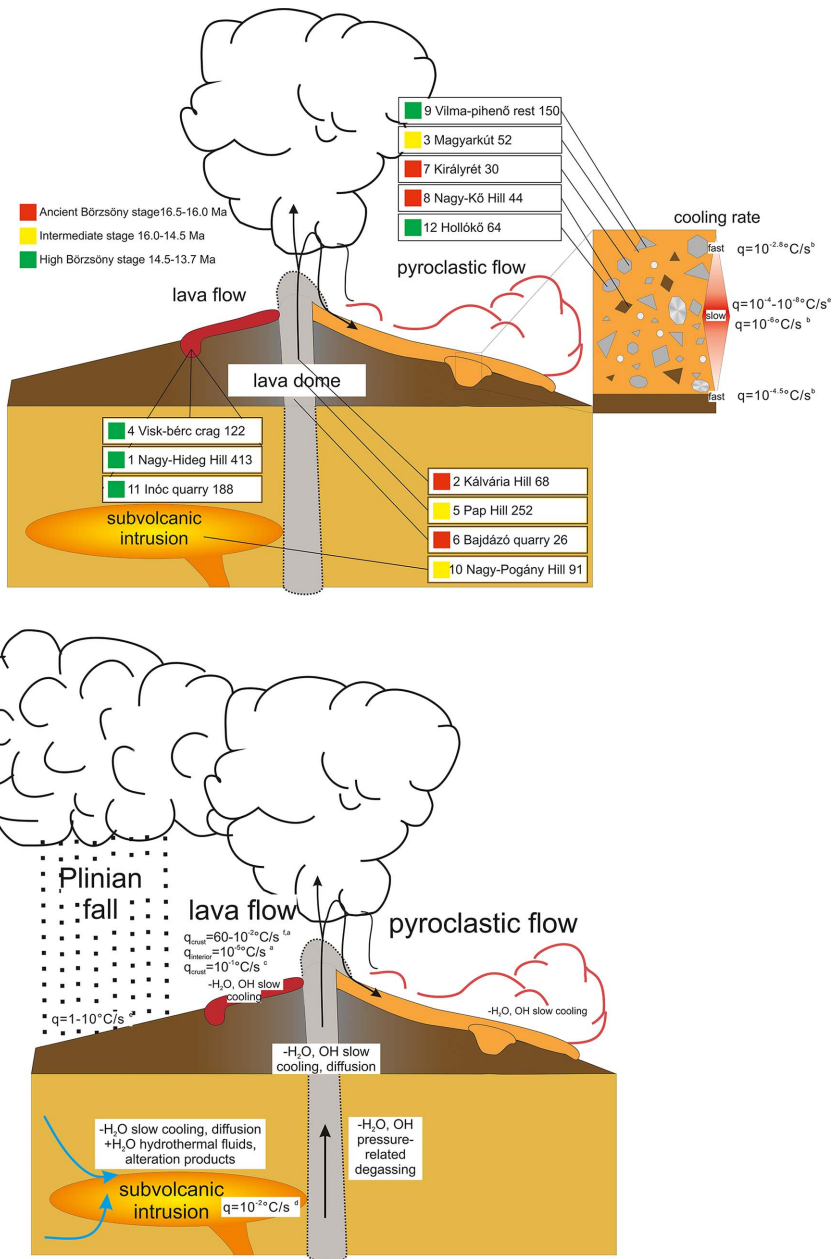


Fig. 7 The relationship between facies, cooling rates, and structural hydroxyl contents. Cooling rates are from the following references indicated by letters in superscript as follows: <sup>a</sup>Coish and Taylor (1979), <sup>b</sup>Ellis et al. (2015), <sup>c</sup>Flynn and Mouginis-Mark (1992), <sup>d</sup>Giordano et al. (2007), <sup>e</sup>Wallace et al. (2003), and <sup>f</sup>Witter and Harris (2007)

show low water content (28 wt. ppm), but this may be also due to hot emplacement and post-eruptive slow cooling, since water content retention depends on clast size (Lloyd et al. 2013) and the height of the sample above the base of the ignimbrite (Biró et al. 2017). Similarly, low water content (43 wt. ppm) is observed in the Magyarkút subaerially deposited lapilli tuff of an ignimbrite sample (no. 3), which was probably caused for the same reasons. The Magyarkút sample belongs to the second volcanic stage, just like sample nos. 5 and 10 (Pap Hill and Nagy-Pogány Hill, respectively). As mentioned, sample no. 5 is part of a lava dome and sample no. 10 could also be considered as a root part of a lava dome or part of a *subvolcanic* body (Fig. 7; Karátson et al. 2000). The petrographic investigations revealed hydrothermally altered mafic components, mostly opacitized or chloritized; in the case of no. 10, Nagy-Pogány Hill, there is altered groundmass, with microholocrystalline texture. Since the hydroxyl content obtained with the “dry” selection is low (29 wt. ppm), we suggest that the earlier water content has been lost due to the aforementioned physical processes or overprinted by the hydrothermal alterations. The “wet” selection’s water content (90 wt. ppm) is about three times the “dry” evaluation’s water content. The main difference between “wet” and “dry” methods is that the “wet” selection allows the contribution of bands belonging to molecular water or alteration products. Thus, the present difference could be also due to the hydrothermal processes affecting the minerals causing entrapment of inclusions.

The sample no. 5 from Pap Hill was also a part of a lava dome, but plagioclase water concentrations are measured to be higher (124 wt. ppm), which could be caused by more moderate post-emplacement diffusional water loss, as it represents the *upper part of a lava dome*. Since, however, the average spectra show observable strong bands at  $\sim 3,620\text{--}3,700\text{ cm}^{-1}$  of hydrous phyllosilicates, the high water content is more likely caused by hydrothermal alteration products of the feldspars. This conclusion is supported by the petrographic features of the phenocrysts.

The samples from the last eruptive period mainly represent basaltic–andesitic and andesitic *lava flows* and subordinate *blocks of pyroclastic breccias* of andesitic and basaltic–andesitic composition. Sample nos. 1, 4, and 11 have high water content (Fig. 7; Nagy-Hideg Hill, Visk-bérc crag, and Inóc quarry; 340, 55, and 155 wt. ppm, respectively); they are from platy, jointed facies of lava flows (Karátson 2007), which could occur near to the surface of the flows, so the water content may be better preserved than that of the massive rocks. However, the spectra also show strong bands that belong to the hydrous phyllosilicates, and are very similar to the plagioclase spectrum of Canyon Flow (YCV-16) presented by Shepherd and Johnson (2016), which they attributed to a hydrothermally altered, fluid inclusion-bearing plagioclase. Based on the spectra, it is more reasonable to propose that there is a significant contribution of molecular water in inclusions. This is verified with the petrography of the plagioclases, where phenocrysts have several zones, with inclusion-rich, spongy cores, and inclusions in certain zones.

The plagioclases of pyroclastic breccias are relatively water-rich in the Vilma-pihenő rest (117 wt. ppm) and water-poorer in the Hollókő breccia (20 wt. ppm; Fig. 7; nos. 9

and 12, respectively). Both samples are from blocks of the breccias, which could have different degassing and cooling history, which affects the retention of water, but since the plagioclase phenocrysts have more inclusions in the Vilma-pihenő rest sample, the higher water content also comes from molecular water content of inclusions.

Since many spectra show intense absorption bands at the region of  $\sim 3,400\text{ cm}^{-1}$ , there is a good reason to assume that the plagioclases may bear nano-inclusions with molecular water content. The unusually high phenocryst water contents can be caused by products of hydrothermal alteration as well (e.g., sericite). The “dry” selecting algorithm provides more realistic, less contaminated data (Fig. 5) to estimate the water content, so the overprinting of water content due to weathering or hydrothermal alterations could be avoided.

### *Magmatic “water” content determination*

Although the measured plagioclase water contents (25–400 wt. ppm) are in good agreement with previously published data (from 12 to 300 wt. ppm; Hamada et al. 2011; Shepherd and Johnson 2016), the accuracy of determining magmatic water contents is disputable because there is currently no directly applicable  $D^{\text{plagioclase/melt}}$  coefficient available for rocks with similar geochemical features to those of Börzsöny (e.g., andesitic and dacitic composition). To obtain a preliminary estimation on the reliability of our measurements, we have calculated with the partitioning coefficient published by Hamada et al. (2013):  $D^{\text{plagioclase/melt}} = 0.008$ . The calculated magmatic water contents are shown in Table 1. The melt water contents in equilibrium are significantly lower (from 0.31 to 4.26 wt.% with the “dry” method), even for mafic-intermediate magmas, than the values constrained with melt-inclusion measurement (e.g., Plank et al. 2013; 4 wt.% average), while intermediate-felsic melts can contain even more up to 10 wt.% water (Petrelli et al. 2018). The differences can be caused by processes, such as hot deposition, long-time magma stalling, and degassing, that the plagioclase phenocrysts have fast diffusion rates, and are subject to syn- and post-eruptive water loss. In an ideal scenario, the plagioclase crystals can inform us about melt water contents in the latest magma storage conditions. Similar conclusions are drawn by Johnson (2005) and Johnson and Rossman (2013) on plagioclase diffusion measurements.

## **Conclusions**

In this study, we have first published plagioclase and magmatic water contents from the Miocene calc-alkaline rocks of CPR: the Börzsöny Mts. Since the “water” content of phenocrysts in a volcanic system has been recognized to play an important role in revealing the evolution of volcanic rocks, this paper also provides a comprehensive review of the magmatic water contents published in the past two decades. This review provides an up-to-date summary about the analytical techniques, concentration

levels, and their implications. Plagioclase phenocrysts from the Börzsöny Mts. were measured with unpolarized micro-FTIR spectroscopy. The water contents (25–400 wt. ppm) of phenocrysts were in better accordance with the cooling history of each sample rather than any other features, such as the mobile trace element contents or An content of plagioclase.

We conclude that the faster diffusion rate of hydrogen might have allowed “water” equilibration in the timescale of hours or days at high temperatures, so the plagioclase water contents are homogenized and can provide information on the syn- and post-eruptive mechanisms that the phenocrysts may have experienced. The homogeneous and irregularly low plagioclase water contents can be explained with processes like (a) re-equilibration in last magma storage or in conduit, syn-eruptively; (b) re-equilibration at the surface or near-surface at lower pressure and higher temperature, allowing post-eruptive diffusive water loss. Due to these processes, there is no direct evidence for the source region’s water content temporal variability, since these processes lead to diffusional water loss or overprinting of initial phenocryst water content. For further research, plagioclase phenocrysts should be collected from facies where the fastest possible cooling is assumed, which in practice means small-sized ash or lapilli from the basal parts of pyroclastic deposits (Lloyd et al. 2013; Biró et al. 2017), and surfaces of subaerial lava flow deposits, which are not altered later.

## **Acknowledgements**

The authors would like to greatly acknowledge Gábor Dobosi for his kind editorial handling, and János Szepesi and Balázs Kiss for their very constructive and careful reviews, which greatly improved the manuscript. This work was supported by ZP’s ÚNKP-17-2 New National Excellence Program of the Ministry of Human Capacities. The volcanological research of TB is supported by the NTP-NFTÖ-18-B-0130 program of the Ministry of Human Capacities. The geochemical investigations of the project were funded by the National Research, Development and Innovation Office of Hungary under the funding scheme of K128122 to IK. Sample preparation facilities were provided by the Hungarian Mining and Geological Survey of Hungary and Eötvös University.

## **References**

- Adam, J., M. Turner, E.H. Hauri, S. Turner 2016: Crystal/melt partitioning of water and other volatiles during the near-solidus melting of mantle peridotite: Comparisons with non-volatile incompatible elements and implications for the generation of intraplate magmas. – *American Mineralogist*, 101, pp. 876–888.
- Aines, R.D., G.R. Rossman 1984: Water in minerals? A peak in infrared. – *Journal of Geophysical Research*, 89, pp. 4059–4071.
- Aubaud, C., H. Bureau, C. Raepsaet, H. Khodja, A.C. Withers, M.M. Hirschmann, D.R. Bell 2009: Calibration of the infrared molar absorption coefficients for H in olivine, clinopyroxene and rhyolitic glass by elastic recoil detection analysis. – *Chemical Geology*, 260/1–2, pp. 286–294.

- Bell, D.R., P.D. Ihinger, G.R. Rossman 1995: Quantitative analysis of trace OH in garnet and pyroxenes. – *American Mineralogist*, 80, pp. 465–474.
- Biró, T., I. Kovács, D. Karátson, R. Stalder, E. Király, G. Falus, T. Fancsik, J. Sándor-Kovács 2017: Evidence for post-depositional diffusional loss of hydrogen in quartz phenocryst fragments within ignimbrites – *American Mineralogist*, 102, pp. 1187–1201.
- Biró, T., I. Kovács, E. Király, G. Falus, D. Karátson, Z. Bendő, T. Fancsik, J. Sándor-Kovács 2016: Concentration of hydroxyl defects in quartz from various rhyolitic ignimbrite horizons: Results from unpolarized micro-FTIR analyses on unoriented phenocryst fragments. – *European Journal of Mineralogy*, 28/2, pp. 313–327.
- Bucholz, C.E., G.A. Gaetani, M.D. Behn, N. Shimizu 2013: Post-entrapment modification of volatiles and oxygen fugacity in olivine-hosted melt inclusions. – *Earth and Planetary Science Letters*, 374, pp. 145–155.
- Burnham, C.W. 1985: Energy release in subvolcanic environments: Implications for breccia formation. – *Economic Geology*, 80/6, pp. 1515–1522.
- Coish, R.A., L.A. Taylor 1979: The effects of cooling rate on texture and pyroxene chemistry in DSDP Leg 34 basalt: A microprobe study. – *Earth and Planetary Science Letters*, 42/3, pp. 389–398.
- Danyushevsky, L.V. 2001: The effect of small amounts of H<sub>2</sub>O on crystallisation of mid-ocean ridge and backarc basin magmas. – *Journal of Volcanology and Geothermal Research*, 110, pp. 265–280.
- Dingwell, D.B. 1996: Volcanic dilemma: Flow or blow? – *Science*, 273, pp. 1054–1055.
- Ellis, B.S., B. Cordonnier, M.C. Rowe, D. Szymanowski, O. Bachmann, G.D.M. Andrews 2015: Groundmass crystallisation and cooling rates of lava-like ignimbrites: The Grey's Landing ignimbrite, Southern Idaho, USA. – *Bulletin of Volcanology*, 77/10, p. 15.
- Flynn, L.P., P.J. Mouginiis-Mark 1992: Cooling rate of an active Hawaiian lava flow from nighttime spectroradiometer measurements. – *Geophysical Research Letters*, 19/17, pp. 1783–1786.
- Gaetani, G.A., T.L. Grove 1998: The influence of water on melting of mantle peridotite. – *Contributions to Mineralogy and Petrology*, 131, pp. 323–346.
- Giordano, D., M. Polacci, A. Longo, P. Papale, D.B. Dingwell, E. Boschi, M. Kasereka 2007: Thermo-rheological magma control on the impact of highly fluid lava flows at Mt. Nyiragongo. – *Geophysical Research Letters*, 34/6, p. 4.
- Giordano, D., J.K. Russell, D.B. Dingwell 2008: Viscosity of magmatic liquids: A model. – *Earth and Planetary Science Letters*, 271/1–4, pp. 123–134.
- Grove, T.L., C.B. Till, M.J. Krawczynski 2012: The role of H<sub>2</sub>O in subduction zone magmatism. – *Annual Reviews of Earth and Planetary Sciences*, 40, pp. 413–439.
- Gyarmati, P. 1976: Vulkanológiai fejlődéstörténet és kőzetgenetika a Börzsöny-hegységben [Volcanological history and petrogenesis in the Börzsöny Mts.]. – *Annual Report of the Geological Institute of Hungary*, 1973, pp. 57–62. (in Hungarian)
- Hamada, M., T. Kawamoto, E. Takahashi, T. Fujii 2011: Polybaric degassing of island arc low-K tholeiitic basalt magma recorded by OH concentrations in Ca-rich plagioclase. – *Earth and Planetary Science Letters*, 308, pp. 259–266.
- Hamada, M., M. Ushioda, T. Fujii, E. Takahashi 2013: Hydrogen concentration in plagioclase as a hygrometer of arc basaltic melts: Approaches from melt inclusion analyses and hydrous melting experiments. – *Earth and Planetary Science Letters*, 365, pp. 253–262.
- Harangi, S.Z., H. Downes, L. Kósa, C.S. Szabó, M.F. Thirlwall, P.R.D. Mason, D. Matthey 2001: Almandine garnet in calc-alkaline volcanic rocks of the northern Pannonian Basin (Eastern–Central Europe): Geochemistry, petrogenesis and geodynamic implications. – *Journal of Petrology*, 42, pp. 1813–1843.
- Harangi, S.Z., H. Downes, M.F. Thirlwall, K. Gméling 2007: Geochemistry, petrogenesis and geodynamic relationships of Miocene calc-alkaline volcanic rocks in the western Carpathian arc, Eastern Central Europe. – *Journal of Petrology*, 48, pp. 2261–2287.
- Hauri, E.H., G.A. Gaetani, T.H. Green 2006: Partitioning of water during melting of the Earth's upper mantle at H<sub>2</sub>O-undersaturated conditions. – *Earth and Planetary Science Letters*, 248, pp. 715–734.

- Johnson, E.A.E. 2005: Magmatic water contents recorded by hydroxyl concentrations in plagioclase phenocrysts from Mount St. Helens, 1980–1981. – Goldschmidt Conference Abstracts, 69, Moscow, ID, USA, p. A743.
- Johnson, E.A.E. 2006: Water in nominally anhydrous crustal minerals: Speciation, concentration, and geologic significance. – *Reviews in Mineralogy and Geochemistry*, 62, pp. 117–154.
- Johnson, E.A.E., G.R. Rossman 2003: The concentration and speciation of hydrogen in feldspars using FTIR and H-MAS-NMR-spectroscopy. – *American Mineralogist*, 88, pp. 901–911.
- Johnson, E.A.E., G.R. Rossman 2004: A survey of hydrous species and concentrations in igneous feldspars. – *American Mineralogist*, 89, pp. 586–600.
- Johnson, E.A.E., G.R. Rossman 2013: The diffusion behavior of hydrogen in plagioclase feldspar at 800–1000 °C: Implications for re-equilibration of hydroxyl in volcanic phenocrysts. – *American Mineralogist*, 98, pp. 1–10.
- Karátson, D. 2007: A Börzsönytől a Hargitáig (From the Börzsöny Mts. to the Harghita Mts.)–Typotex Kiadó, Budapest, 463 p. (in Hungarian)
- Karátson, D., E. Márton, S.Z. Harangi, S. Józsa, K. Balogh, Z. Pécskay, S. Kovácsvölgyi, G. Szakmány, A. Dulai 2000: Volcanic evolution and stratigraphy of the Miocene Börzsöny Mountains, Hungary: An integrated study. – *Geologica Carpathica*, 51, pp. 325–343.
- Karátson, D., I. Oláh, Z. Pécskay, E. Márton, S.Z. Harangi, A. Dulai, T. Zelenka 2007: Miocene volcanism in the Visegrád Mountains, Hungary: An integrated approach and regional implications. – *Geologica Carpathica*, 58, pp. 541–563.
- Korpás, L., E. Csillag-Teplánszky, G. Hámor, L. Ódor, I. Horváth, U. Fügedi, S.Z. Harangi 1998: Magyarázó a Börzsöny és Visegrádi-hegység földtani térképéhez, 1:50 000 [Explanations for the Geological Map of the Börzsöny and the Visegrád Mountains, 1:50 000]. – Geological Institute of Hungary, Budapest, 216 p. (in Hungarian)
- Korpás, L., B. Lang 1993: Timing of volcanism and metallogenesis in the Börzsöny Mountains, Northern Hungary. – *Ore Geological Review*, 8, pp. 477–501.
- Kovács, I., J. Hermann, H.S.C. O'Neill, J.F. Gerald, M. Sambridge, G. Horváth 2008: Quantitative absorbance spectroscopy with unpolarized light, Part II: Experimental evaluation and development of a protocol for quantitative analysis of mineral IR spectra. – *American Mineralogist*, 93/5–6, pp. 765–778.
- Kovács, I., C.S. Szabó 2008: Middle Miocene volcanism in the vicinity of the Middle Hungarian Zone: Evidence for an inherited enriched mantle source. – *Journal of Geodynamics*, 45, pp. 1–17.
- Le Bas, M.J., R.W. Le Maitre, A. Streckeisen, B. Zanettin 1986: A chemical classification of volcanic rocks based on the total alkali-silica diagram. – *Journal of Petrology*, 27, pp. 745–750.
- Le Voyer, M., P.D. Asimow, J.L. Mosenfelder, Y. Guan, P.J. Wallace, P. Schiano, J.M. Eiler 2014: Zonation of H<sub>2</sub>O and F concentrations around melt inclusions in olivines. – *Journal of Petrology*, 55/4, pp. 685–707.
- Libowitzky, E., G.R. Rossman 1997: An IR Absorption calibration for water in minerals. – *American Mineralogist*, 82, pp. 1111–1115.
- Liu, J., Q. Xia, E. Deloule, H. Chen, M. Feng 2015: Recycled oceanic crust and marine sediment in the source of alkali basalts in Shandong, Eastern China: Evidence from magma water content and oxygen isotopes. – *Journal of Geophysical Research: Solid Earth*, 120, pp. 8281–8303.
- Lloyd, A.S., E. Ferriss, P. Ruprecht, E.H. Hauri, B.R. Jicha, T. Plank 2016: An assessment of clinopyroxene as a recorder of magmatic water and magma ascent rate. – *Journal of Petrology*, 57/10, pp. 1865–1886.
- Lloyd, A.S., T. Plank, P. Ruprecht, E.H. Hauri, W. Rose 2013: Volatile loss from melt inclusions in pyroclasts of differing sizes. – *Contributions to Mineralogy and Petrology*, 165, pp. 129–153.
- McDonough, W.F., S.S. Sun 1988: A primitive mantle composition from xenoliths. – *Chemical Geology*, 70/1–2, pp. 12–112.
- Mosenfelder, J.L., G.R. Rossman, E.A.E. Johnson 2015: Hydrous species in feldspars: A reassessment based on FTIR and SIMS. – *American Mineralogist*, 100, pp. 1209–1221.
- Nakamura, N. 1974: Determination of REE, Ba, Fe, Mg, Na and K in carbonaceous and ordinary chondrites. – *Geochimica et Cosmochimica Acta*, 38, pp. 757–775.

- Nazzareni, S., M. Pompilio, H. Skogby, P.F. Zanazzi 2008: Water contents of pyroxenes from Etna recent eruptions. – AGU Fall Meeting Abstracts, San Francisco, pp. V21B–2109.
- Nazzareni, S., H. Skogby, P.F. Zanazzi 2011: Hydrogen content in clinopyroxene phenocrysts from Salina mafic lavas (Aeolian Arc, Italy). – *Contributions to Mineralogy and Petrology*, 162, pp. 275–288.
- O’Leary, J.A., G.A. Gaetani, E.H. Hauri 2010: The effect of tetrahedral Al<sup>3+</sup> on the partitioning of water between clinopyroxene and silicate melt. – *Earth and Planetary Science Letters*, 297, pp. 111–120.
- Ochs, F.A., R.A. Lange 1999: The density of hydrous magmatic liquid. – *Science*, 283, pp. 1314–1317.
- Okumura, S. 2011: The H<sub>2</sub>O content of andesitic magmas from three volcanoes in Japan, inferred from the infrared analysis of clinopyroxene. – *European Journal of Mineralogy*, 23, pp. 771–778.
- Pécskay, Z., J. Lexa, A. Szakács, I. Seghedi, K. Balogh, V. Konečný, T. Zelenka, M. Kovács, T. Póka, A. Fülöp, E. Márton, C. Panaiotu, V. Cvetkovic 2006: Geochronology of Neogene magmatism in the Carpathian arc and intra-Carpathian area. – *Geologica Carpathica*, 57, pp. 511–530.
- Petrelli, M., K.E. Omari, L. Spina, Y. Le Guer, G. La Spina, D. Perugini 2018: Timescales of water accumulation in magmas and implications for short warning times of explosive eruptions. – *Nature Communications*, 9, Article 770.
- Plank, T., K. Kelley, M. Zimmer, E. Hauri, P.J. Wallace 2013: Why do mafic arc magmas contain ~4 wt% water on average? – *Earth and Planetary Science Letters*, 364, pp. 168–179.
- Portnyagin, M., R. Almeev, S. Matveev, F. Holtz 2008: Experimental evidence for rapid water exchange between melt inclusions in olivine and host magma. – *Earth and Planetary Science Letters*, 272/3–4, pp. 541–552.
- Rossmann, G.R. 2006: Analytical methods for measuring water in nominally anhydrous minerals. – *Reviews in Mineralogy and Geochemistry*, 62/1, pp. 1–28.
- Sambridge, M., J.F. Gerald, I. Kovács, H.S.C. O’Neill, J. Hermann 2008: Quantitative absorbance spectroscopy with unpolarized light. Part I: Physical and mathematical development. – *American Mineralogist*, 93, pp. 751–764.
- Saunders, A.D., M.J. Norry, J. Tarney 1991: Fluid influence on the trace-element compositions of subduction zone magmas. – *Philosophical Transactions of the Royal Society of London, Series A*, 335, pp. 377–392.
- Seghedi, I., H. Downes, A. Szakács, P.R.D. Mason, M.F. Thirlwall, R. Emilian, Z. Pécskay, E. Márton, C. Panaiotu 2004: Neogene–Quaternary magmatism and geodynamics in the Carpathian-Pannonian region: A synthesis. – *Lithos*, 72/3–4, pp. 117–146.
- Shepherd, H.V., E.A.E. Johnson 2016: Water contents of yellowstone magmas estimated from hydroxyl concentrations in feldspar phenocryst. – *Geological Society of America Abstracts with Programs*, Boulder, CO, 40, p. 62.
- Sparks, R.S.J. 2003: Dynamics of magma degassing. – In: Oppenheimer, C., D. M. Pyle, J. Barclay (Eds): *Volcanic degassing*. Geological Society, London, Special Publications, 213, pp. 5–22.
- Turner, M., S. Turner, N. Mironov, M. Portnyagin, K. Hoernle 2017: Can magmatic water contents be estimated from clinopyroxene phenocrysts in some lavas? A case study with implications for the origin of the Azores Islands. – *Chemical Geology*, 466, pp. 436–445.
- Wade, J.A., T. Plank, E.H. Hauri, K.A. Kelley, K. Roggensack, M. Zimmer 2008: Prediction of magmatic water contents via measurement of H<sub>2</sub>O in clinopyroxene phenocrysts. – *Geology*, 36, pp. 799–802.
- Wallace, P.J. 2005: Volatiles in subduction zone magmas: Concentrations and fluxes based on melt inclusion and volcanic gas data. – *Journal of Volcanology and Geothermal Research*, 140, pp. 217–240.
- Wallace, P.J., J. Dufek, A.T. Anderson 2003: Cooling rates of Plinian-fall and pyroclastic-flow deposits in the bishop tuff: Inferences from water speciation in quartz-hosted glass inclusions. – *Bulletin of Volcanology*, 65, pp. 105–123.
- Weis, F.A., H. Skogby, V.R. Troll, F.M. Deegan, B. Dahren 2015: Magmatic water contents determined through clinopyroxene: Examples from the Western Canary Islands, Spain. – *Geochemistry Geophysics Geosystems*, 16, pp. 2127–2146.
- Witter, J.B., A.J. Harris 2007: Field measurements of heat loss from skylights and lava tube systems. – *Journal of Geophysical Research: Solid Earth*, 112, p. B01203.